

Mid-Holocene thinning of David Glacier, Antarctica: Chronology and Controls

Jamey Stutz¹, Andrew Mackintosh², Kevin Norton³, Ross Whitmore^{1,2}, Carlo Baroni⁴, Stewart S.R. Jamieson⁵, R. Selwyn Jones², Greg Balco⁶, Maria Cristina Salvatore⁴, Stefano Casale⁴, Jae Il Lee⁷, Yeong Bae Seong⁸, Robert Mckay¹, Lauren J. Vargo¹, Daniel Lowry^{1,9}, Perry Spector⁶, Marcus Christl¹⁰, Susan Ivy Ochs¹⁰, Luigia Di Nicola¹¹, Maria Iarossi⁴, Finlay Stuart¹¹, and Tom Woodruff¹²

¹Antarctic Research Centre, Victoria University of Wellington, PO Box 600, Wellington, New Zealand 6140

²School of Earth, Atmosphere and Environment, Monash University, 14 Rainforest Walk, Victoria, Australia 3800

³School of Geography, Earth and Environmental Sciences, Victoria University of Wellington, PO Box 600, Wellington, New Zealand 6140

⁴Dipartimento di Scienze della Terra, Università di Pisa, Via Santa Maria, 53, 56126 Pisa, Italy

⁵Department of Geography, Durham University, South Road, Durham, DH1 3LE, UK

⁶Berkeley Geochronology Center, 2455 Ridge Road, Berkeley, CA 94709, USA

⁷Korean Polar Research Institute, 26 Songdomirae-ro, Yeonsu-gu, Incheon 21990, Korea

⁸Department of Geography, Korea University, 145 Anam-ro, Seongbuk-gu, Seoul, Korea

⁹GNS Science, 1 Fairway Dr. Avalon, 5010, New Zealand

¹⁰Department of Physics, ETH Zürich, Otto-Stern-Weg 5 8093 Zürich, Switzerland

¹¹Scottish Universities Environmental Research Centre, Scottish Enterprise Technology Park/Rankine Av, Glasgow G75 0QF, United Kingdom

¹²PRIME Lab, Purdue University 525 Northwestern Avenue, West Lafayette, IN 47907, USA

Correspondence: Jamey Stutz (jamey.stutz@vuw.ac.nz)

Abstract. Quantitative satellite observations provide a comprehensive assessment of ice sheet mass loss over the last four decades, but limited insights into long-term drivers of ice sheet change. Geological records can extend the observational record and aid our understanding of ice sheet – climate interactions. Here we present the first millennial-scale reconstruction of David Glacier, the largest East Antarctic outlet glacier in Victoria Land. We use surface exposure dating of glacial erratics deposited 5 on nunataks to reconstruct changes in ice **thickness** through time. We then use numerical modelling experiments to determine the drivers of glacial thinning.

Thinning profiles derived from $45\ ^{10}\text{Be}$ and ^3He surface exposure ages show that David Glacier experienced rapid thinning up to 2 m/yr during the mid-Holocene (\sim 6,500 years ago). Thinning stabilised at 6 kyr, suggesting initial formation of the Drygalski Ice Tongue at this time. Our work, along with terrestrial cosmogenic nuclide records from adjacent glaciers, shows 10 simultaneous glacier thinning in this sector of the Transantarctic Mountains occurred \sim 3 kyr after the retreat of marine- based grounded ice in the western Ross Embayment. The timing and rapidity of the reconstructed thinning at David Glacier is similar to reconstructions in the Amundsen and Weddell embayments.

In order to identify the potential causes of these rapid changes along the David Glacier, we use a glacier flow line model 15 designed for calving glaciers and compare modelled results against our geological data. We show that glacier thinning and marine-based grounding line retreat is initiated by interactions between enhanced sub-ice shelf melting and reduced lateral

buttressing, leading to Marine Ice Sheet Instability. Such rapid glacier thinning events are not captured in continental or sector-scale numerical modelling reconstructions for this period. Together, our chronology and modelling suggest a \sim 2,000-year period of dynamic thinning in the recent geological past.

Copyright statement. Creative Commons Attribution 4.0 License

20 1 Introduction

The Earth experienced its last major period of climate warming between \sim 20,000 and 11,700 years ago. During this period known as the Last Glacial Termination, ice sheets retreated in both hemispheres, causing a sea level rise of \sim 130 m. Ice sheet retreat continued into the Holocene, and global sea level stabilised at near preindustrial levels by 6-7,000 years ago. During this period, the Antarctic Ice Sheet (AIS) retreated from expanded positions on the continental shelf. Ice sheet thinning and 25 retreat was rapid at times, potentially contributing to periods of rapid sea level rise (Weber et al., 2014). However, constraints, and particularly quantitative age control on this retreat behaviour are only available for a limited number of sites in Antarctica, and are entirely absent from David Glacier, the largest outlet glacier in Victoria Land and the focus of this study. Improved understanding of the timing and the processes that caused AIS retreat during this period help us to better understand the processes driving observed mass loss in parts of Antarctica today.

30 Geological reconstruction of the AIS through time provides critical insights into the history of ice sheet change and can narrow uncertainty on Antarctica's contribution to global sea level rise during this period. A geologic perspective on ice sheet behavior is particularly useful as:

1. Quantitative satellite observations only extend back \sim 40 years (IMBIE, 2018; IPCC, 2013; Miles et al., 2013; Rignot et al., 2019) and these observations do not fully capture natural variability of ice sheet behaviour.
2. Integration of the data constraining marine extent and terrestrial thickness of an ice mass through time provides a robust data set for evaluation of numerical ice sheet model simulations, which are used to predict future ice sheet contributions to sea level rise.
3. Data from the Gravity Recovery and Climate Experiment (GRACE) satellites offer a powerful measure of present-day ice sheet mass change but require a correction for millennial to centennial-scale ice sheet load history. This is because the 40 gravity signal is strongly influenced by crustal uplift from glacio-isostatic adjustment (GIA) (Whitehouse et al., 2012; Whitehouse, 2018). Solutions using GRACE gravity data, corrected using a precise GIA signal, have the capability to provide a more accurate estimate of present-day ice sheet mass balance at a regional scale (King et al., 2012; Simms et al., 2019).
4. Examples of past ice sheet changes provide evidence of the climatic processes and dynamic feedbacks by which ice sheets respond to environmental forcing. For example, the mass balance of large, marine-terminating outlets of Antarctica

is affected by decadal to interannual changes in regional climate drivers such as the Southern Annular Mode and El Niño-Southern Oscillation (Dutrieux et al., 2014; Miles et al., 2013; Walker and Gardner, 2018; Assmann et al., 2019; Wille et al., 2019). However, we do not currently know if these short-term drivers are important over centennial to millennial timescales.

50 Reconstructions of large marine terminating outlet glaciers provide an opportunity to constrain and understand the terrestrial and marine sectors of ice sheets. At the LGM, the David Glacier thickened and expanded as an ice stream, coalesced with grounded marine-based ice, and extended hundreds of kilometres into the western Ross Sea (Anderson et al., 2014; Livingstone et al., 2012; Shipp et al., 1999). During deglaciation, grounding line retreat from north of Coulman Island was initiated by ~13 ka, with retreat near Terra Nova Bay by ~11 ka (Licht et al., 1996; Domack et al., 1999; McKay et al., 2008). Subsequent 55 grounding line retreat north of Ross Island was achieved by ~8.6 ka and a modern configuration established by ~2-4 ka (Anderson et al., 2014; McKay et al., 2016). Outlet and valley glaciers along the Northern Victoria Land sector (Reeves, Priestley, and Tucker, Aviator, Campbell glaciers, respectively) began thinning at ~17 ka and the majority of thinning ceased by ~7.5 ka, broadly coincident with a linear rise in sea level and ocean temperatures throughout deglaciation (Baroni and Hall, 2004; Johnson et al., 2008; Smellie et al., 2018; Goehring et al., 2019; Rhee et al., 2019). In contrast, outlet glaciers covering 60 a large swath of the Transantarctic Mountains (TAM) from Southern Victoria Land to Southern TAM, experienced episodic thinning during the early-mid Holocene, likely due to local topographic effects associated with Marine Ice Sheet Instability (MISI) (Jones et al., 2015; Spector et al., 2017). Overall, variation in the timing of glacier thinning suggests sea-level rise, ocean warming, and overdeepened subglacial topography as general controls for the reconstructed glacier behaviour.

The David Glacier drains the East Antarctic Ice Sheet (EAIS), traverses and incises the TAM and discharges into the western 65 Ross Sea as the floating Drygalski Ice Tongue, first discovered by the British National Antarctic Expedition (1901-1904) (Fig. 1 and S1). Comprising an area ~210,000 km², the glacier is the largest in Victoria Land, representing a significant element of the Antarctic cryosphere, draining from Dome C and Talos Dome. Given its size and inferred intimate connection with the marine-based grounded ice in the Ross sea highlights the David Glacier as a key target for further investigation. Through 70 surface exposure dating of glacial deposits, this study aims to constrain the LGM to present behaviour of the David Glacier. Further, we investigate the relative role of ocean heat and lateral buttressing on glacier thinning and retreat through idealised glacier flowline modelling experiments. **We use geologic data and ice sheet model outputs to frame and inform sensitivity experiments with our basin scale flowline model, building on previous successful implementations of this approach (Jones et al., 2015; Whitehouse et al., 2017).**

2 Methods

75 2.1 Field and laboratory methods

Surface exposure dating using *in situ* terrestrial cosmogenic nuclides has transformed the ability to reconstruct the AIS through time (e.g. Stone et al., 2003; Mackintosh et al., 2007; Todd et al., 2010; Balco, 2011; White et al., 2011; Jones et al., 2015;

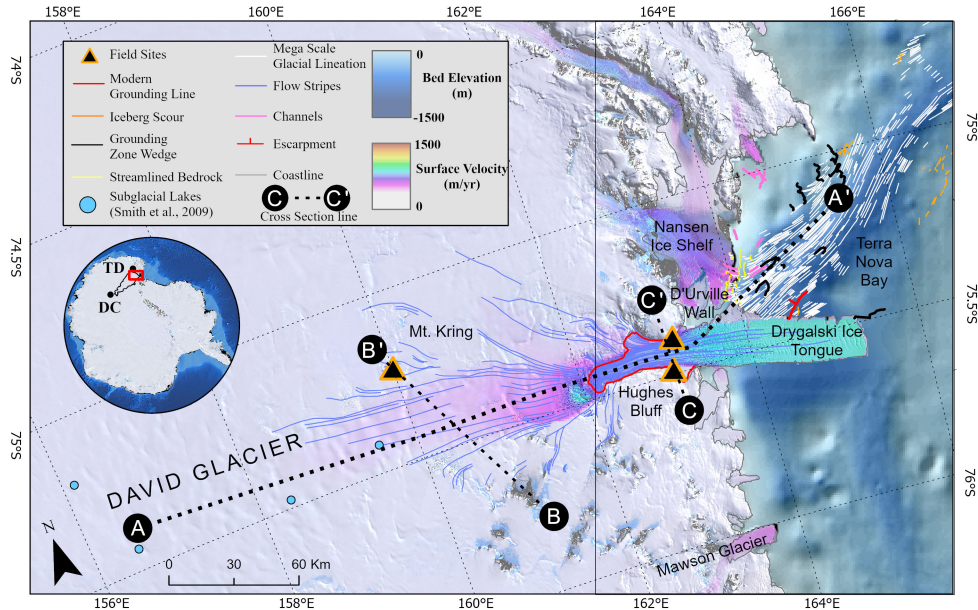


Figure 1. Map of greater David Glacier/Terra Nova Bay region including mapped sub-marine geomorphic features and geographic features mentioned in text. Geomorphic cross sections (A-A', B-B' and C-C') highlighted in Fig. S1. Inset shows extent of main map along with drainage basin of David Glacier and position of two local ice domes (Dome C (DC) and Talos Dome (TD)). Data sources: Satellite imagery of (Bindschadler et al., 2008), surface velocity of (Rignot et al., 2011), surface elevation of (Howat et al., 2019), bed elevation of (Fretwell et al., 2013) and bathymetry of (Arndt et al., 2013)

Spector et al., 2017; Small et al., 2019). In the field, we collected erratics and rocky outcrops adjacent to the David Glacier both upstream and downstream of the present-day grounding line. Downstream sites are expected to show the most recent and dramatic change while sites upstream are expected to record smaller and longer term changes in ice thickness (Anderson et al., 2004; Bockheim et al., 1989). Using the structure from motion technique (Vargo et al., 2017), we use helicopter based photography to construct a high-resolution digital elevation model of each field site allowing integration of glacial geological field surveys with the regional and local geomorphology (Baroni et al., 2004) (Figs.S3 and S4). Sampling focused primarily on glacial erratic cobbles from local glacial deposits and glacially moulded bedrock surfaces which were collected along vertical 80 transects perpendicular to the modern glacial flow direction. Faceted and striated glacial erratics are preferred as they indicate subglacial origins with minimal post-depositional erosion. The aim of the sampling method is to track the upper ice surface and dramatic change while sites upstream are expected to record smaller and longer term changes in ice thickness (Anderson et al., 2004; Bockheim et al., 1989). Using the structure from motion technique (Vargo et al., 2017), we use helicopter based 85 photography to construct a high-resolution digital elevation model of each field site allowing integration of glacial geological field surveys with the regional and local geomorphology (Baroni et al., 2004) (Figs.S3 and S4). Sampling focused primarily on glacial erratic cobbles from local glacial deposits and glacially moulded bedrock surfaces which were collected along vertical transects perpendicular to the modern glacial flow direction. Faceted and striated glacial erratics are preferred as they indicate subglacial origins with minimal post-depositional erosion. The aim of the sampling method is to track the upper ice surface through time (Stone et al., 2003; Mackintosh et al., 2007; Jones et al., 2015; Small et al., 2019).

Of the 110 samples collected in the field, 36 samples were processed for ^{10}Be analysis and 9 samples for ^3He analysis. For ^{10}Be analysis, quartz is the target mineral and is present in granites and sandstones. In this case, sandstones are preferred as

90 they contain ~90% quartz and require significantly less physical processing. In the field, we preferentially sampled on isolated, local topographic high points, distant from areas of blue ice, snow drifts or local till deposits. While it is the focus of this study to use glacial erratics to track glacier thinning, **we also collected bedrock samples to better understand the longer term burial and exposure histories due to non-erosive burial by cold-based ice (Atkins, 2013; Joy et al., 2014).**

95 Samples collected in the field were processed at the cosmogenic nuclide facilities at Te Herenga Waka Victoria University of Wellington. For ^{10}Be , we separated quartz by crushing and sieving to extract the 250-500-micron grain size fraction. Magnetic minerals were separated using a Frantz isodynamic magnetic separator. For granitic rocks, feldspars were removed by froth flotation. We etched samples for one day in 10% Hydchloric acid, for one day in 2.5% Hydroflouric acid (HF) and a 3 days in 1%HF to further purify the quartz separates. Beryllium was extracted from quartz following an established method including addition of ^9Be carrier, enhanced quartz etching and digestion followed by ion exchange column chemistry and 100 BeOH precipitation (Norton et al., 2008). Targets of BeO were packed and sent to the PRIME lab for analysis using accelerated mass spectroscopy (AMS). For ^3He , we targeted pyroxene from the 125-250 micron grain size fraction. Pure pyroxene was obtained using an established HF etching method and $^3\text{He}/^4\text{He}$ ratios were measured at the Berkeley Geochronology Center noble gas spectrometer (Bromley et al., 2014; Blard et al., 2015; Balter-Kennedy et al., 2020). We supplemented this data set with eight samples collected prior to the 2016-17 austral summer and those samples were processed for ^{10}Be or ^3He using 105 methods outlined in Oberholzer et al. (2003, 2008); Di Nicola et al. (2009, 2012). Exposure ages are calculated by converting the AMS derived $^{10}\text{Be}/^9\text{Be}$ ratio to ^{10}Be concentration by subtracting a known amount of ^9Be carrier added during chemical processing. Final exposure ages are calculated using ^{10}Be or ^3He concentration, field information (elevation, shielding, and sample thickness) and production rate scaling method (LSDn) (Balco et al., 2008; Lifton et al., 2014; Marrero et al., 2016; Jones et al., 2019). For ^{10}Be , we employed Jones et al. (2019) systematics (<http://ice-tea.org/en/>) and for ^3He , we use Balco 110 et al. (2008) systematics (<https://hess.ess.washington.edu/>). All relevant data used to calculate exposure ages are served on the ICE-D online database (Balco, 2020) within the David Glacier region (antarctica.ICE-D.org) **and in supplemental data tables 2-6. The resulting glacier thinning chronologies derived from surface exposure ages inform our glacier modelling approach by providing geometric targets for evaluating the simulated maximum thickness of ice, and the subsequent magnitude and duration of ice surface thinning.**

115 2.2 Glacier modelling approach

In order to understand potential controls on the grounding line migration and onshore thinning, we apply a glacier flow-line model to the David Glacier. Originally designed to track grounding line migration using a moving grid, the flow-line model we employ has been described fully elsewhere (e.g. Vieli and Payne (2005); Nick et al. (2009); Jamieson et al. (2012); Enderlin et al. (2013); Jamieson et al. (2014); Clason et al. (2016); Whitehouse et al. (2017)). The underlying theory and governing 120 equations are outlined in Vieli and Payne (2005) and here we describe the components pertinent to our research questions.

The glacier modelling focuses on a ~1,600 km long flowline covering a diverse set of flow regimes from the higher-elevation, low-velocity Dome C area to the lower-elevation, high-velocity outlet glacier (David Glacier), ice shelf (Drygalski Ice Tongue)

and ice stream beyond where, in the past, it converged with grounded ice in the Ross Sea. Ice flow is modelled as a mechanically coupled ice sheet, ice stream and ice shelf flow governed by fundamental equations 1 - 6.

125 Ice sheet flow **along the ice sheet interior, u** , is calculated using the shallow ice approximation which assumes ice flow only from internal ice deformation and horizontal velocity defined as:

$$u = C \left(\frac{\delta s}{\delta x} \right) h^{n+1} \quad (1)$$

where $n (=3)$ is Glens flow law exponent, s is ice surface elevation, h is ice thickness and C is a constant given by:

$$C = \frac{2A(\rho_i g)^n}{n+2} \quad (2)$$

130 As ice reaches flotation, ice is assumed to spread unidirectionally along the flowline, ice shelf flow is balanced by:

$$2 \frac{\delta}{\delta x} h v \frac{\delta u}{\delta x} = \rho_i g h \frac{\delta s}{\delta x} \quad (3)$$

where ρ_i is ice density (0.910 g/cm³), g is gravitational acceleration (9.8 m/s) and v is the vertically average effective viscosity defined as:

$$v = A^{\frac{-1}{n}} \left[\left(\frac{\delta u}{\delta x} \right)^2 \right]^{(1-n)(2n)} \quad (4)$$

135 Where A is the temperature dependant rate factor (for -20°C) and $\frac{\delta u}{\delta x}$ is the effective strain rate.

For an ice stream, equation 4 is modified by including a basal friction coefficient β which is linearly related to the horizontal velocity u and is given by:

$$2 \frac{\delta}{\delta x} h v \frac{\delta u}{\delta x} - \beta^2 u = \rho_i g h \frac{\delta s}{\delta x} \quad (5)$$

Recent applications using this model include testing the impact of a width term to calculate lateral buttressing along a 140 coupled ice stream-shelf and enhanced treatment of ice shelf dynamics. Nick et al. (2010) and Jamieson et al. (2012) modelled depth (H) and width (W) averaged ice flow (u) using the following equation:

$$2 \frac{\delta}{\delta x} h v \frac{\delta u}{\delta x} - \beta^2 u + \frac{H}{W} \left(\frac{5u}{2AW} \right)^{\frac{1}{n}} = \rho_i g h \frac{\delta s}{\delta x} \quad (6)$$

The inclusion of the width term allows modelling of changing offshore trough width which is common in palaeo-ice streams and outlet glaciers, and further supported by geomorphic interpretations using high resolution bathymetry data (Jamieson 145 et al., 2012; Livingstone et al., 2012, 2016). **For this study, we map all geomorphic features using the global multi-resolution**

topography data set within GeoMapApp (geomapapp.org) based on analogs (Dowdeswell et al., 2016) and prior regional mapping (Stutz, 2012; Shipp et al., 1999; Anderson et al., 2014; Halberstadt et al., 2016).

Whitehouse et al. (2017) improved the ice shelf dynamics to incorporate the treatment of large horizontal grounding line movements that are expected for the palaeo-David Glacier based on the long term presence of the Drygalski Ice Tongue 150 and evidence of extensive sub-ice shelf conditions inferred from marine sedimentary cores (Domack et al., 1999; McKay et al., 2008). In the model, the ice shelf geometry evolves with time, and variations in ice shelf thickness and extent are fed into lateral drag calculations (Whitehouse et al., 2017). Improved treatment of ice shelf dynamics allows exploration of the grounding line sensitivity to ice shelf feedbacks such as reduced lateral buttressing. Importantly for this study, a reduction in lateral buttressing is expected as the expanded David Glacier and grounded ice in the Ross Sea decouple, which has been 155 suggested from interpretation of submarine geomorphic features in the western Ross Sea (Shipp et al., 1999; Halberstadt et al., 2016).

2.2.1 Boundary conditions

The model domain, ~~sampled at 5 km resolution~~, runs along a \sim 1,600 km flowline from Dome C to the continental shelf break (Fig. 2 and Fig. S6). ~~Fig 1 and Fig. S1 provide map extent of cross section views detailing the subglacial topography 160 surrounding the modern day grounding line.~~ The marine sector of the flowline follows the Drygalski Trough axis and runs parallel to mapped mega-scale glacial lineations (MSGL). ~~Using standard basin delineation tools in ArcGIS, we construct a drainage basin outline from surface elevation and ice velocity (Rignot et al., 2011; Howat et al., 2019).~~ In order to simplify the flowline domain, we focus on the dominant ice stream emanating from Dome C. Together with the flowline (centre of ice stream), we use these basin outlines to construct an ice stream-parallel width across the onshore domain. Offshore, we 165 determine ice stream width by orientation and distribution of trough parallel MSGLs consistent with Jamieson et al. (2012).

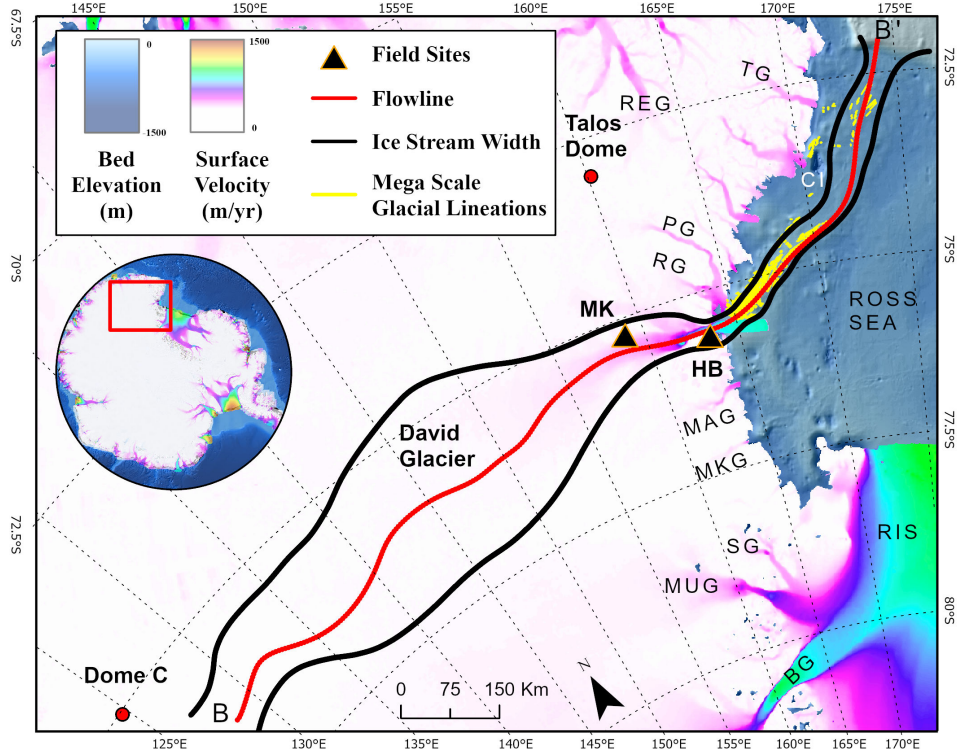


Figure 2. Map of model domain with modern ice surface velocity of (Rignot et al., 2011) and bathymetry of Arndt et al. (2013). Flowline follows red line, ice stream width in black. RIS: Ross Ice Shelf, BG: Byrd Glacier, MUG: Mulock Glacier, SG: Skelton Glacier, MKG: Mackay Glacier, MAG: Mawson Glacier, RG: Reeves Glacier, PG: Priestley Glacier, AG: Aviator Glacier TG: Tucker Glacier, CI: Coulman Island, HB: Hughes Bluff, MK: Mt. Kring

In order to evaluate model performance and appropriate boundary conditions for deglacial experiments, we conduct sensitivity experiments designed to reproduce the modern behaviour of the David Glacier. The model allows the user to input surface and bed geometry, ice stream width, accumulation, velocity and a basal traction parameter. Modern surface elevation, accumulation and ice velocity are well constrained from satellite and *in situ* measurements (Rignot et al., 2011; van Wessem et al., 170 2018; Howat et al., 2019). In order to account for confluent ice from tributary glaciers we employ an ice mass accumulation scheme used in previous modelling studies whereby tributary ice mass is added along the length of the ice stream (Jamieson et al., 2014). This tributary ‘injection’ from a secondary ice stream originating from Talos Dome is included in the surface mass budget and for the David Glacier model domain.

Ongoing aerogeophysical and remote sensing techniques continue to reveal new detail of the subglacial environment of the 175 AIS (Morlighem et al., 2019). Common among many TAM outlet glaciers, a prominent bedrock high immediately upstream of the modern grounding line provides a significant stabilising impact on the David Glacier (Fretwell et al., 2013; Morlighem

et al., 2019). The bed geometry along the flowline is derived solely from Bedmap2 and the International Bathymetric Chart of the Southern Ocean (Fretwell et al., 2013; Arndt et al., 2013).

Geologic data from former glaciated terrains and satellite observations can be used to approximate basal conditions, yet a general lack of *in situ* data from the ice sheet basal environment lead to enduring uncertainties in the basal stress regime (Joughin et al., 2006; Stokes et al., 2015). Based on existing knowledge of sea floor morphology and consistent with previous modelling experiments, the basal traction parameter used in this model attempts a first order approximation of two subglacial basal environments: 1) relatively high basal traction for onshore ice flow over bedrock and 2) relatively low basal traction for offshore ice flow over soft sediments associated with basal till deposits (Dowdeswell et al., 2004; O Cofaigh et al., 2005).

Modern day sensitivity experiments tune user defined parameters such as internal ice temperature and basal traction parameters until best-fit with modern surface geometry. Overall, the modern grounding line position, ice shelf thickness and ice shelf length are stable over a 2,000 year modelled period. The model is unable to reproduce stable conditions along the steep surface profile as the David Glacier descends from the ice sheet interior. In this zone, the modelled upper surface is steep and undergoes thinning throughout the modelled time period. In an effort to stabilise the upper surface upstream of the grounding line, we tune the basal traction parameter, effectively stiffening the bed, to reduce the modelled instability. Resultant modelled estimates of basal shear stress approach 100 kPa in this setting. While difficult to constrain with *in situ* measurements, Zoet et al. (2012) suggest higher stresses should be expected near the modern day grounding zone which is consistent with the modelled stress distribution in this study.

2.2.2 Deglaciation approach

LGM geometric boundary conditions incorporate modelled ice thickness and surface velocity from W12, a geologically constrained continental scale glacial isostatic adjustment model (Fig.S6) (Whitehouse et al., 2012). Using the W12 modelled ice thickness and modern bed elevation (Fretwell et al., 2013) allows for an estimate of ice surface elevation without introducing uncertainty involving variable along flow isostatic response and dynamic topography associated with the long-term evolution of the Antarctic subglacial topography (Stern et al., 2005; Whitehouse et al., 2019; Paxman et al., 2019). **We do not compare our sensitivity experiments results with those of W12, we purely use a derived upper ice surface as a starting point for our model during spin up. The resulting ice surface elevation geometrically fits to geologic data (i.e. covers highest elevation Holocene aged erratics) and serves as an initial ice profile for deglaciation sensitivity experiments. Further, it is not the intention of these sensitivity experiments to reproduce the exact timing of marine-based grounding line retreat, but model results provide insights to the dominant processes responsible for glacier thinning and retreat.**

In order to account for environmental changes during deglaciation, transient changes in accumulation and internal ice temperature are tuned over the modelled period to ensure a stable LGM configuration consistent with geological constraints. Knowledge of past accumulation over glacial-interglacial cycles are restricted to ice core data and internal ice sheet layer mapping near high elevation ice domes (Siegert, 2003; Frezzotti et al., 2005; Buiiron et al., 2011; Cavitte et al., 2018). Generally, modern accumulation patterns show relatively low accumulation (0.02 m/yr) over the East Antarctic interior and high accumulation (0.2 m/yr) near the coastline (Arthern et al., 2006; Lenaerts et al., 2012; van Wessem et al., 2018). Interpretations

from ice core records suggest LGM accumulation rates were lower than modern accumulation rates and generally correlate well with temperature proxy records throughout the Holocene (Siegert, 2003; Veres et al., 2013). We use a scaling relationship between modern accumulation patterns and suggest that accumulation at ~ 15 ka was roughly 75% of modern accumulation (Veres et al., 2013).

215 Deglacial sensitivity experiments designed to understand the controls on thinning and retreat are initialised with a set of user defined parameters derived from modern sensitivity experiments. Using an optimised set of accumulation and temperature forcings, we explore transient changes in lateral buttressing and sub-ice shelf melt rate to isolate their relative influence on glacier thinning and retreat. **Lateral buttressing and sub-ice shelf melt rate are the only two forcings we investigate as regional proxies for internal ice temperature and accumulation (only two other user defined forcings for this model) are poorly constrained and show relatively minor variation over this period (Buiron et al., 2011; Verleyen et al., 2011).** Finally, we initiate 220 grounding line retreat by progressively increasing sub-ice-shelf melt rate or decreasing lateral buttressing.

All sensitivity experiments run for 15 kyr with an initial spin up period lasting 7.5 kyr, at which point a forcing perturbation is applied. When forcing the model, we linearly increase the forcing over a 500 year period. In sub-ice-shelf melt cases, we varied the sub-ice-shelf melt rate perturbation within a 0.5 m/yr window in order to simulate short-lived pulses of relatively 225 warmer or cooler water mass changes. All idealised scenarios are presented along with results in Supplementary Table S1.

3 Results - chronology

Of the 45 samples analysed in this study, 21 yield mid-Holocene exposure ages. Holocene aged samples are interpreted to have received minimal prior exposure (i.e inheritance) and suggest a simple exposure history. Focusing on two sites, we derive a high-resolution chronology of glacier thinning from Mt. Kring and Hughes Bluff.

230 3.1 Mt. Kring

Mt. Kring, situated in the interior of the EAIS, lies along the flank of the ice stream draining Dome C. The nunatak, composed of layered dolerite, rises ~ 300 metres above the local ice surface. Of the 24 samples processed, three are dolerite bedrock and 21 erratics of mixed lithologies (Fig. 3 and S3). The surface at the peak of Mt. Kring lacks glacial striations or erratics and has an apparent ${}^3\text{He}$ bedrock exposure age of 554 ± 91 ka. A discontinuous, steep ridge line between ~ 200 -300 metres 235 above local ice was not sampled due to inaccessibility. At ~ 200 metres above the local ice, the bedrock is striated parallel to modern ice flow direction and has an apparent ${}^3\text{He}$ exposure age of 550 ± 82 ka. The highest elevation erratic is found at ~ 180 metres above the local ice with increasing erratic abundance culminating in a drift sheet covering nearly all bedrock below 240 ~ 110 metres above local ice. Striated, bulletted cobbles and boulders of dolerite, basalt and sandstone are common in the thin, patchy drift covering the bedrock. The glacial drift is composite in age and we identify three populations of erratic exposure ages (Fig. 4A). The younger population spans from 7.4-5.5 ka (${}^{10}\text{Be}$, n=5)(Fig. 4B). The older population spans from 51-25 ka (${}^{10}\text{Be}$, n=8 and ${}^3\text{He}$, n=4). The oldest erratic age population shows scattered evidence of glacial behavior between 123-63 ka

(^{10}Be , n=2, ^3He , n=2). The older populations are likely an artifact of repeated burial by overriding ice and multiple periods of exposure (i.e. inheritance).

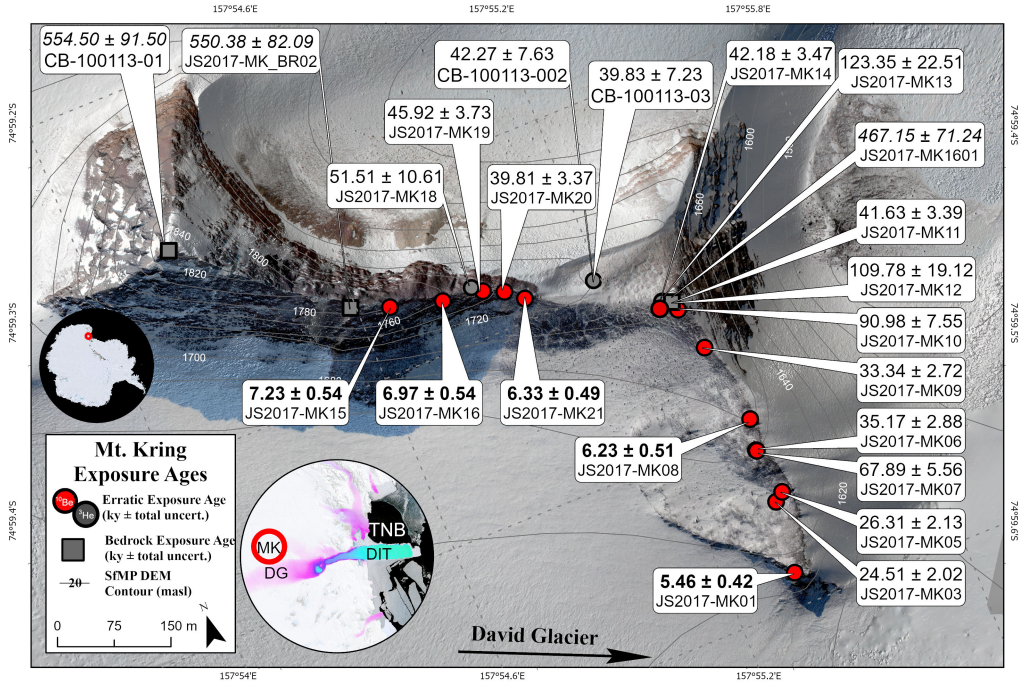


Figure 3. Orthomosaic map of Mt. Kring with all exposure ages, ^{10}Be (red) and ^3He (grey), and total errors. Erratics and bedrock ages plotted as circles and squares, respectively. Large inset displays surface velocity of (Rignot et al., 2011) and small inset displays LIMA data of (Bindschadler et al., 2008). DG=David Glacier, DIT=Drygalski Ice Tongue, TNB=Terra Nova Bay and MK=Mt. Kring

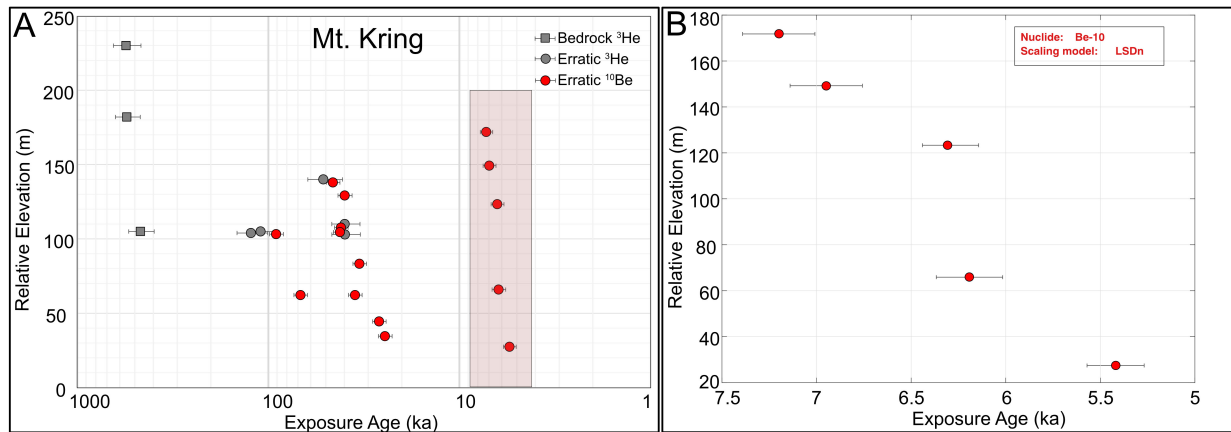


Figure 4. Calculated surface exposure ages for Mt. Kring. (A) All exposure ages. Erratics plotted as circles, bedrock as squares (^{10}Be , red and ^3He , grey). Errors bars show total uncertainty. (B) Shows only Holocene ages.

3.2 Hughes Bluff

245 Hughes Bluff, situated on the Scott Coast, is a granite outcrop along the southern flank of the David Glacier. The outcrop is glacially scoured exhibiting spectacular roches moutonnées, crescentic gouge marks and striations parallel to modern flow directions (Fig. 5 and Fig. S4). Scattered glacial erratics blanket the entire outcrop. ^{10}Be exposure ages from 15 erratics span from 6.7-4.3 ka (Fig. 6). The majority of glacial erratics are dated to between 6.7 and 6.2 ka. Two bedrock surface exposure ages from the highest and lowest outcrops ($20.55 \text{ ka} \pm 2.10$, $5.5 \pm 0.47 \text{ ka}$) suggest significant wet-based glacial erosion

250 during the LGM. At 20 metres above local ice, similar bedrock and erratic ages provide evidence of recent emergence of this lower outcrop since 5.5 ka. Given the extensive glacial erosion, the LGM surface elevation at this site was likely considerably greater than 230m, the maximum elevation at Hughes Bluff. While the onset and magnitude of thinning prior to 6.7 ka is poorly constrained, the Hughes Bluff chronology indicates a period of rapid ice surface lowering during the mid-Holocene.

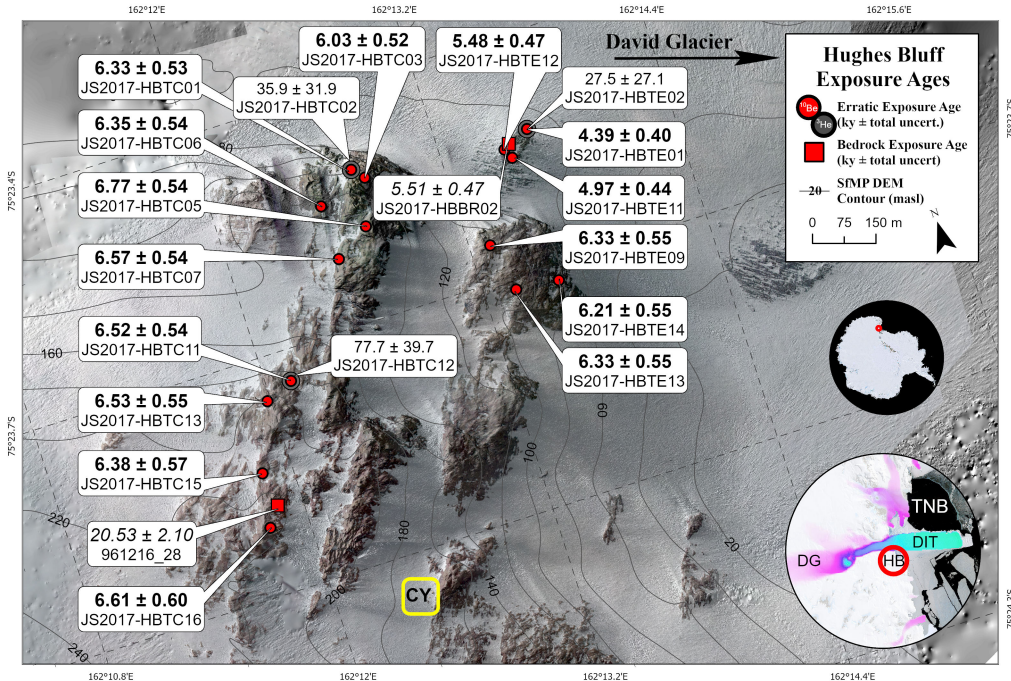


Figure 5. Orthomosaic map of Hughes Bluff with all exposure ages, ^{10}Be (red) and ^{3}He (grey), and total errors listed. Erratics and bedrock ages plotted as circles and squares, respectively. Large inset shows surface velocity of (Rignot et al., 2011) and small inset shows LIMA data of (Bindschadler et al., 2008). DG=David Glacier, DIT=Drygalski Ice Tongue, TNB=Terra Nova Bay, HB=Hughes Bluff and CY=Camp Yellow

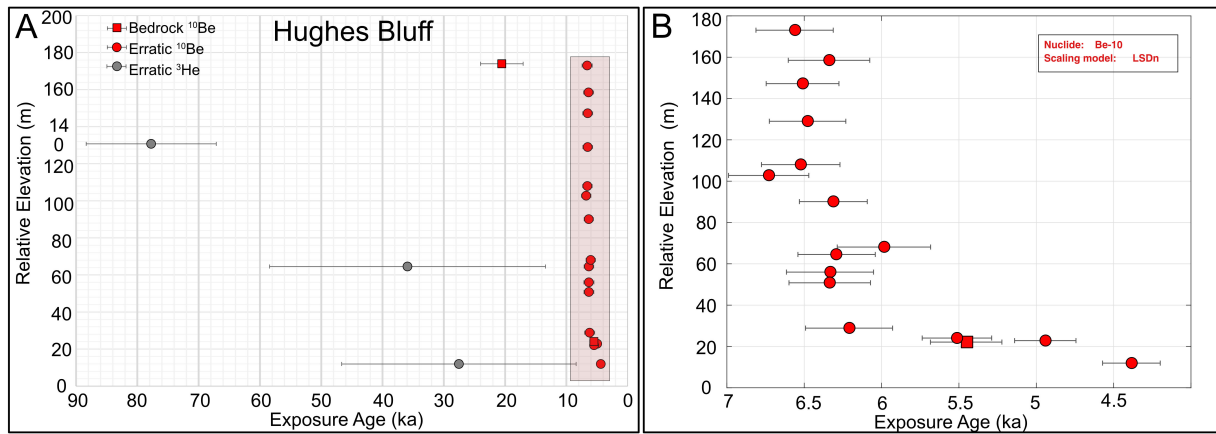


Figure 6. Calculated surface exposure ages for Hughes Bluff (A) All exposure ages. Erratics plotted as circles, bedrock as squares (^{10}Be , red) and ^{3}He , grey). Errors bars show total uncertainty. (B) Shows only Holocene ages.

3.3 High elevation constraints

255 In an effort to identify higher elevation glacial activity and long-term erosion history, field work was undertaken along the D'Urville Wall and Mt. Neumayer area (Fig. S5). The D'Urville Wall is a steep, high-elevation (>400 m) granite outcrop delimiting the northern flank of David Fjord. The geomorphology and exposure ages from two field sites situated high above the David Glacier (Mt. Neumayer and Cape Phillipi) limit the reconstruction of the upper glacier surface during the LGM. Mt. Neumayer extending above the D'Urville Wall forms a rounded summit with faint striations sub-parallel to modern ice flow
 260 with few scattered erratics. In areas above 400 m, bedrock samples contain weathering rinds and deep weathering pits filled with erratics (Baroni et al., 2004; Giorgetti and Baroni, 2007). Bedrock exposure ages from Mt. Neumayer (649 metres above local ice, 642 ± 61 ka), a terrace on top of the D'Urville Wall (418 metres above local ice, 116 ± 10 ka) and Cape Phillipi (~ 300 metres above local ice, 532 ± 52 ka, 957 ± 98 ka) suggest either a thin cover of cold based ice or ice free conditions through the LGM. High elevation bedrock samples are much younger than exposure ages from nearby bedrock at similar height above
 265 the local ice surface and suggests burial by non-erosive ice (Di Nicola et al., 2012). Together with the geomorphic evidence from Hughes Bluff, bedrock exposure ages from the northern flank of David Glacier constrain the LGM upper surface between 300-649 metres above the local ice surface, broadly consistent with ~ 400 masl derived from LGM age drift deposits in Terra Nova Bay (Stuiver et al., 1981; Orombelli et al., 1990; Di Nicola et al., 2009) (Fig. S2).

3.4 Palaeo-thinning rates

270 Using the high-resolution chronology from Hughes Bluff and Mt. Kring, we derive a mean estimate of past thinning rates along David Glacier using a weighted least squares regression scheme within the iceTEA plotting tools (www.ice-tea.org) (Jones et al., 2019). These reconstructed glacier thinning rates are compared to modern thinning rates derived from satellite data and continent scale ice sheet models (Small et al., 2019). At Mt. Kring, we reconstruct a longer and slower thinning

event from 7.5-5.5 ka of up to 0.19 m/yr (0.06-0.19, 2σ) (Fig. 7A). At Hughes Bluff, we reconstruct a period of rapid thinning 275 320 from 6.7-6.2 ka of up to 2 m/yr (0.19-2.06 m/yr, 2σ) followed by \sim 4 kyr period of minimal thinning (Fig. 7B). The reconstructed palaeo-thinning along the David Glacier during the mid-Holocene is synchronous with rapid thinning reconstructed at a number of sites in Antarctica (Nichols et al., 2019; Johnson et al., 2019; Small et al., 2019; Bentley et al., 2017; Spector et al., 2017; Jones et al., 2015; Johnson et al., 2014; Todd et al., 2010; Stone et al., 2003). However, the rate of paleo thinning 280 reconstructed at Hughes Bluff is one of the highest rates recorded in Antarctica, comparable to a reconstruction from nearby Mackay Glacier (Small et al., 2019; Jones et al., 2015).

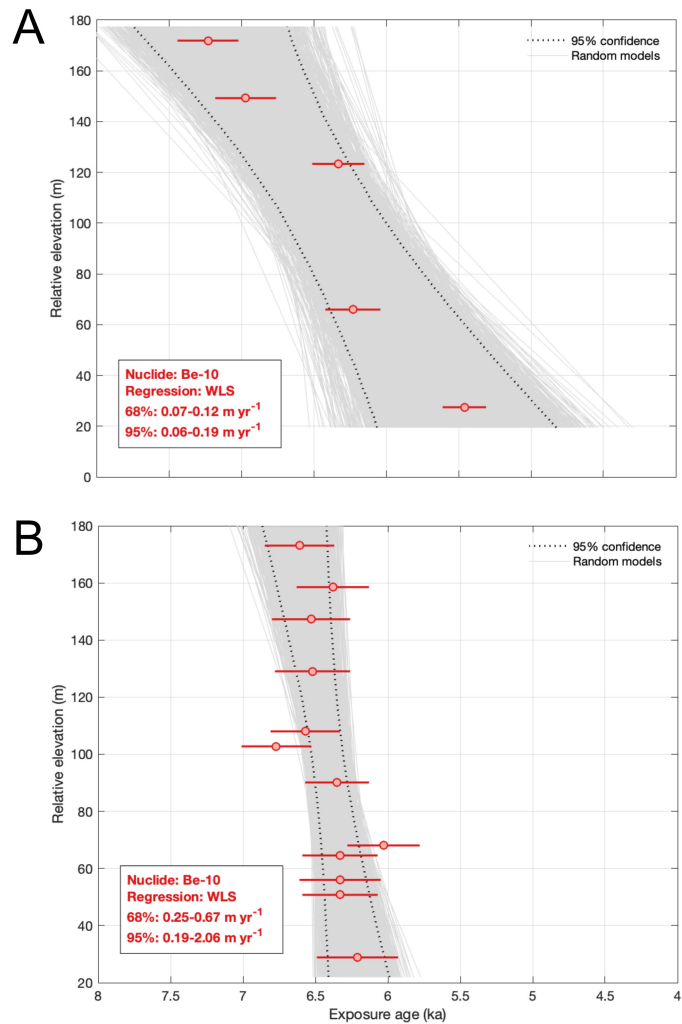


Figure 7. Linear thinning rates estimated for mid-Holocene records using ice-tea.org from (Jones et al., 2019) for: A) Mt. Kring Holocene samples, B) Hughes Bluff samples with outliers identified and omitted using outlier detection in ice-tea.org.

The variation in thinning rates between Mt. Kring and Hughes Bluff is suggestive of past dynamic thinning rather than accumulation-driven outlet glacier changes. Previous work from inland sites similar to Mt Kring suggested that such sites changed little or may have thickened during the Holocene due to accumulation increases (Bockheim et al., 1989; Denton et al., 1989). In contrast, the synchronous timing but smaller magnitude of thinning observed at Mt Kring in this study suggest that 285 this thinning was driven by ice sheet processes at the coast that propagated inland. Such dynamic thinning, where increased ice-shelf basal melting and grounding line retreat leads to accelerated flow and inland thinning, is well documented along modern marine terminating margins of the Greenland and Antarctic ice sheets (Pritchard et al., 2009, 2012), yet identification in geologic record is rare, primarily due to a lack of exposed bedrock in the upper reaches of glacier catchments. The thinning 290 history from David Glacier allows for a unique comparison with the broad pattern of dynamic thinning derived from the modern satellite record and suggests dynamic thinning can occur >100km into the interior of the EAIS and can persist over multi-millennial timescales.

3.5 Exposure age data - ice sheet model comparison

During the LGM, ice core records and numerical model outputs suggest that the ice sheet experienced widespread thinning in its interior, while coastal sites experienced extensive thickening (Verleyen et al., 2011; Mackintosh et al., 2014). Our data from 295 Mt Kring show that the ice sheet was thicker at this site during the LGM, and recorded ~200 metres of thinning during the Holocene. This provides a critical tie point between the high elevation, low accumulation ice domes where ice cores are drilled and the low elevation, high accumulation coastal sites with more abundant geologic data. Mt. Kring is the first site along the high elevation margin of the EAIS to constrain LGM ice sheet behavior and represents a unique site to compare with other ice sheet reconstructions and continental-scale ice sheet modelling experiments.

300 The chronologies from David Glacier provide critical insights in which to compare against modelled reconstructions from continent-scale ice sheet models. Using the data-model comparison software (dmc.ICE-D.org), we extracted a modelled elevation history for David Glacier from five different forward ice sheet models (four continental-scale and one regional-catchment scale) and one prescriptive post-glacial rebound model (Argus et al., 2014; Pollard et al., 2016, 2017, 2018; Kingslake et al., 2018; Lowry et al., 2019). This suite of ice sheet models, in which we compare against our geologic data, represents variation 305 in model grid size, flow approximations, model physics used, forcing and boundary conditions. We use these to provide a reasonable first order approximation for expected results from the ice sheet modelling community. Further, in order to overcome differences in spatial resolution, the scheme extracts an interpolated ice elevation history from the model grid cell containing the field site and its neighbouring model grid cell.

310 The resulting data-model comparison for Hughes Bluff and Mt. Kring reveal a noticeable mismatch in time during the main phase of thinning (Fig. 8). For Mt. Kring, ice sheet models indicate a phase of thinning that precedes our thinning history by ~4-7 kyr. For Hughes Bluff, the timing lag is comparable to Mt. Kring with one notable exception being the post glacial rebound model of ICE-6G. This improved match is likely because ICE-6G is constrained by multiple relative sea level curves along the Scott Coast (Baroni and Hall, 2004; Hall, 2009; Argus et al., 2014). The style of thinning is variable between models with noticeable short-lived pauses in thinning, mainly during the Antarctic Cold Reversal (~15-13 ka) (Pedro et al., 2016).

315 For Mt. Kring, the magnitude of modelled elevation change matches well with the surface exposure age data. As discussed
 previously, the Hughes Bluff chronology likely captures only part of the full thinning history. Overall, the data-model mismatch
 may be related to (1) individual topographic features/outcrops not being spatially resolved in the models, (2) limited constraints
 on ocean/atmosphere forcing which impact rate of retreat (e.g. Lowry et al., 2019) and (3) poorly constrained model parameters
 that influence basal sliding, isostatic adjustment and ice flow/rheology which impact the rate of ice sheet response to a climate
 320 forcing (Lowry et al., 2020; Kingslake et al., 2018).

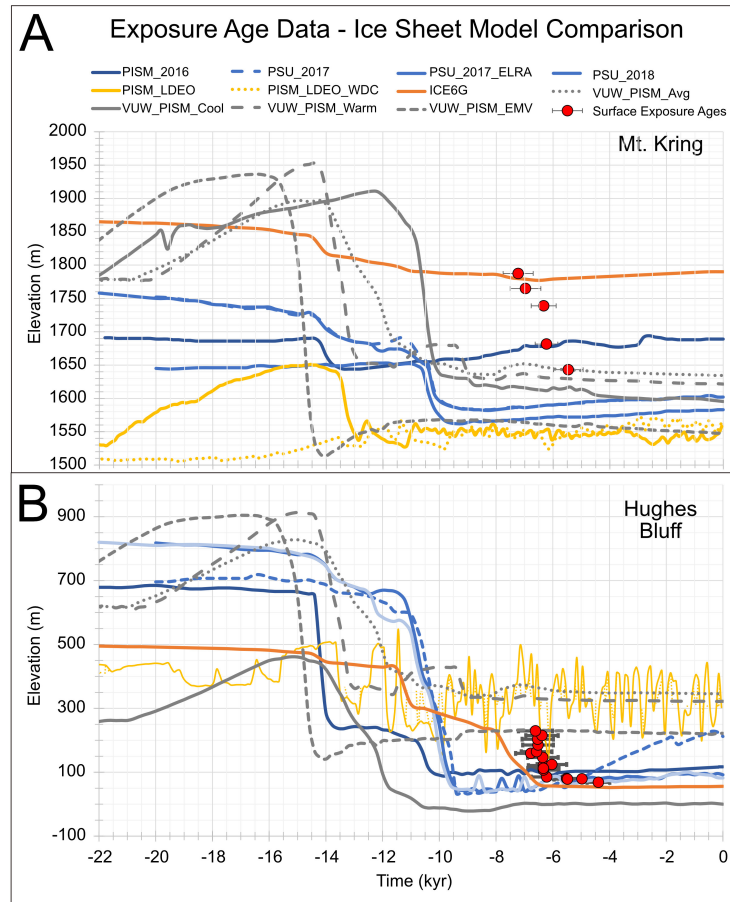


Figure 8. Surface exposure age data - ice sheet model comparisons for a) Mt. Kring and b) Hughes Bluff. Ice sheet modelled reconstruction data and supporting information from dmc.ice-d.org

4 Results - Deglacial sensitivity experiments

Based on the above chronologies, the main episode of glacier thinning occurs during the mid-Holocene and captures >200 metres of glacier change along the David Glacier. This time period does not correlate with significant increases in atmospheric temperature or global mean sea level (e.g. (Lambeck et al., 2014; Menzel et al., 2011; Liu et al., 2009), therefore, we ask:

325 1) What is the role of ocean heat in driving the observed glacier thinning and retreat? and 2) Given the inferred intimate link between the expanded David Glacier and grounded ice in the Ross Sea, what impact does ice sheet buttressing have on the timing and style of glacier thinning and retreat? The style and rate of modelled thinning and retreat from all experiments are compiled in Table S1. **While we do not force our simulations by any date specific reconstructions or proxy data, we co-view our model results against our geologic data to allow generalised time-varying geometric relationships to be compared.**

330 Focusing solely on sub-ice shelf melt rate, a set of sensitivity experiments (M1-3) simulate the impacts of enhanced ocean heat on grounding line retreat (Fig. 9). **For these experiments, we progressively increased melt rate until partial to full retreat is initiated. Threshold values represent this step-wise increase in sub-ice shelf melt rate.** After a 7.5 kyr spin up period, a threshold sub-ice shelf melt rate of -11 m/yr achieves rapid grounding line retreat behaviour and is consistent with the modern grounding line position. For melt rates between -2 and -10 m/yr, grounding line retreat is rapid but the final grounding line remains pinned 335 to the prominent sill at the mouth of the David Fjord. Modelled surface reconstructions place the upper ice surface \sim 300 metres above the Hughes Bluff site, yet agree well with Mt. Kring data constraints. In the high melt case (M3), the grounding line position stabilises at the sill for approximately 5 kyr. The final retreat phase from the sill to a modern position correlates with a final surface consistent with modern observations.

340 Focusing on lateral buttressing reduction experiments (S1-3), we simulate the impacts of glacier-ice sheet decoupling on grounding line retreat, **a scenario suggested from glacial geomorphic features in the western Ross Sea (Shipp et al., 1999; Halberstadt et al., 2016)** (Fig. 10). After a 7.5 kyr model spin up period, ice shelf buttressing is incrementally reduced until retreat is initiated. Retreat occurs when lateral buttressing is reduced by 4%. Further ice shelf debuttressing by 40% retreats the modelled grounding line to near modern configuration, deep in the David Fjord. In both cases, the reduced buttressing forces 345 rapid grounding line retreat to a prominent sill at the mouth of the David Fjord. In these scenarios, the resulting modelled upper ice surface remains above the Hughes Bluff site when pinned to the sill. At Mt. Kring, modelled rapid thinning is synchronous with Hughes Bluff yet results in an unrealistic final surface elevation 100s of metres below observed modern surface elevation.

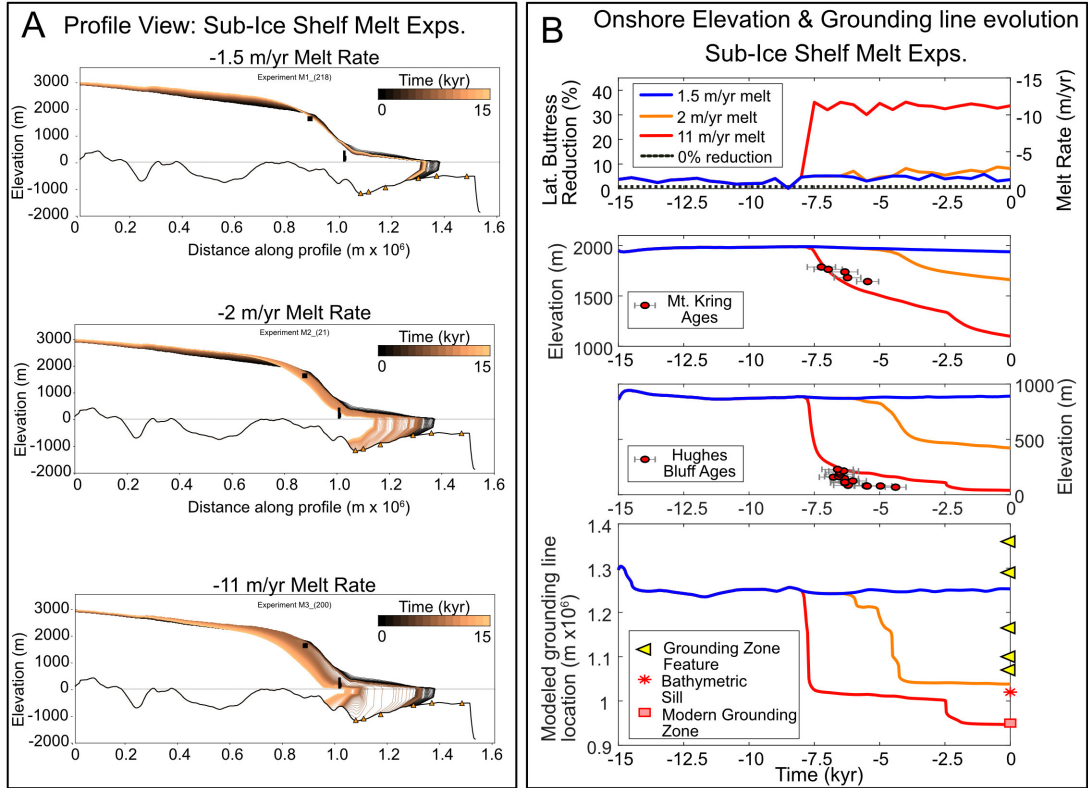


Figure 9. A) Profile View: 15 kyr evolution of modelled upper ice surface along flowline for sub-ice shelf melt rate experiments. Black bars represent elevation range from three sites in this study. Orange triangles represent offshore features marking observed grounding zone wedges. B) Onshore elevation and grounding line evolution for sub-ice shelf melt rate experiments. Top panel: Forcings applied, Top middle panel: Time-transgressive elevation profile for Mt. Kring with exposure ages, bottom middle panel: Time-transgressive elevation profile for Hughes Bluff surface exposure ages, and lower panel: Evolution of grounding line position with modern grounding line position, bathymetric sill at mouth of David Fjord and mapped grounding zone features.

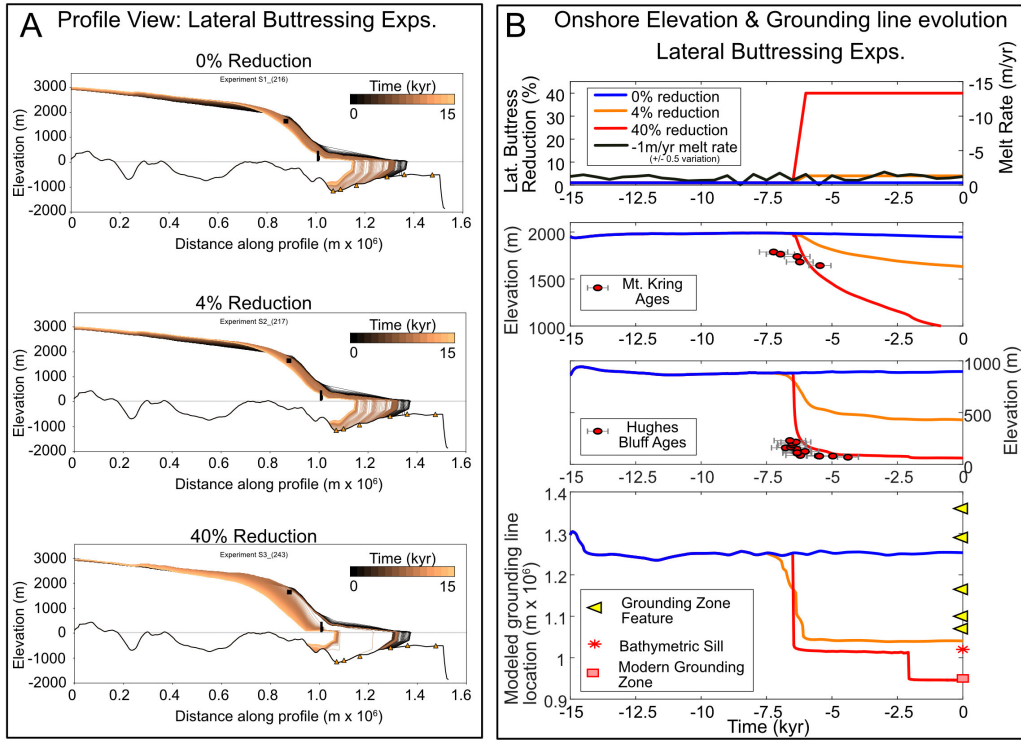


Figure 10. A) Profile View: 15 kyr evolution of modelled upper ice surface along flowline for lateral buttressing experiments. Black bars represent elevation range from three sites in this study. Orange triangles represent offshore features marking observed grounding zone wedges. B) Onshore elevation and grounding line evolution for lateral buttressing experiments. Top panel: Forcings applied, Top middle panel: Time-transgressive elevation profile for Mt. Kring with exposure ages, bottom middle panel: Time-transgressive elevation profile for Hughes Bluff surface exposure ages, and lower panel: Evolution of grounding line position with modern grounding line position, bathymetric sill at mouth of David Fjord and mapped grounding zone features.

Overall when forcings are combined, lower threshold values are required to initiate thinning and retreat (Fig. 11). Modelled upper ice surface reconstruction agrees well with the Mt. Kring chronology, yet Hughes Bluff remains ice covered until grounding line retreat from the sill approximately 5-6 kyr after the main phase of thinning and retreat.

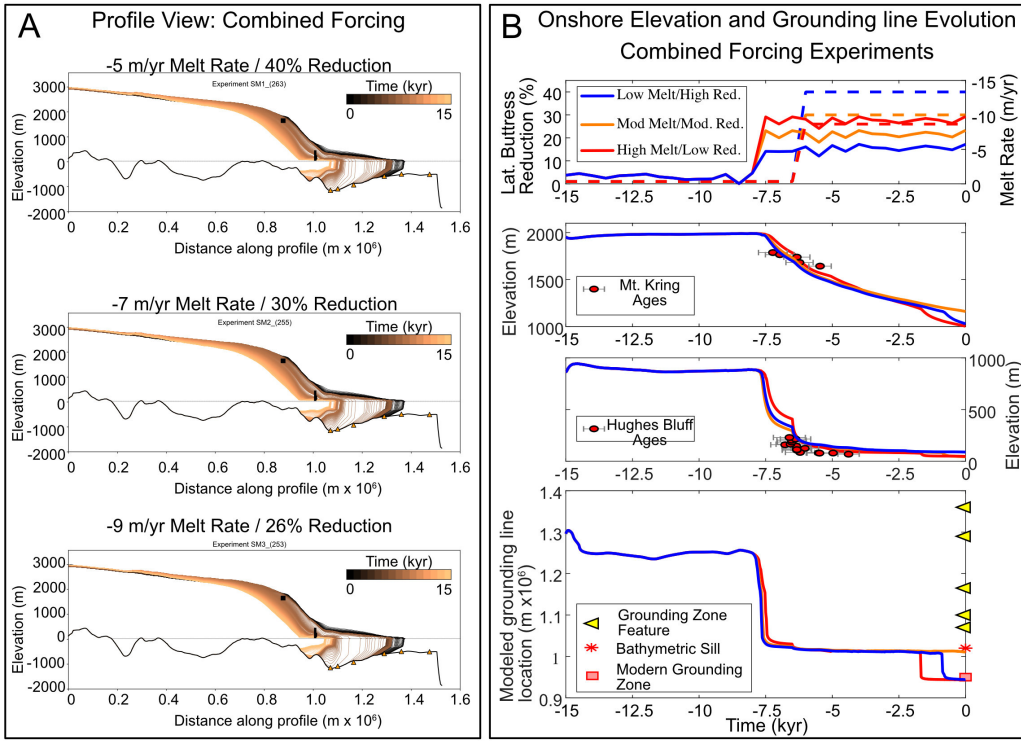


Figure 11. A) Profile View: 15 kyr evolution of modelled upper ice surface along flowline for combined forcing experiments. Black bars represent elevation range from three sites in this study. Orange triangles represent offshore features marking observed grounding zone wedges. B) Onshore elevation and grounding line evolution for lateral buttressing experiments. Top panel: Forcings applied, Top middle panel: Time-transgressive elevation profile for Mt. Kring with exposure ages, bottom middle panel: Time-transgressive elevation profile for Hughes Bluff surface exposure ages, and lower panel: Evolution of grounding line position with modern grounding line position, bathymetric sill at mouth of David Fjord and mapped grounding zone features.

350 We are confident that our modelling results reasonably reconstruct the period of multi-millennial glacial change during
 351 the mid-Holocene. However our approach does have limitations including imperfect knowledge of past boundary conditions;
 352 treating ice as isothermal; lack of isostasy and meltwater parameterization; and no use of a calving law to control ice shelf
 353 length. Through modern sensitivity experiments, geologic control on geometry and a general fit to modern sub-ice shelf melt
 354 rates and basal stress, we remain confident our results support a first order approximation for the dominant controls on the
 355 David Glacier's thinning history.

5 Discussion

The thinning history of David Glacier places modern observations in a long-term perspective and allows for local, regional and continent-wide comparisons with other glacial histories and modelled ice sheet reconstructions. High-resolution, low-

inheritance exposure ages obtained from Hughes Bluff and Mt. Kring overlap in time, yet reveal different thinning styles with
360 Hughes Bluff recording rapid ice surface lowering, and Mt. Kring revealing a much slower thinning signal. The chronology from Mt. Kring implies glacier thinning reached far inland along zones of streaming ice and provides rare constraints on ice behaviour from the margins of the EAIS.

The results of flow line modelling experiments along the expanded David Glacier reveal a threshold-driven sensitivity to both sub-ice shelf melt rate and ice stream lateral buttressing. Periods of modelled grounding line retreat match periods of onshore
365 thinning constrained by surface exposure studies at two locations along the flowline. The results show the glacier response occurs at lower threshold values when the processes act in combination, consistent with previous applications of this model (Jamieson et al., 2014). **Although the sensitivity experiments are inconclusive as to which process or combination of processes forced the observed onshore thinning, we discuss potential explanations relating to the thinning profile at Hughes Bluff and the data-model mismatch at Mt. Kring.**

370 5.1 Terrestrial-marine reconstruction

During the LGM, outlet glaciers and grounded ice thickened and expanded to the continental shelf edge surrounding Antarctica (Livingstone et al., 2012; Anderson et al., 2014; Bentley et al., 2014). Since the LGM, the onshore thinning varied spatially, but occurred primarily during the Holocene ((Small et al., 2019). Along the Transantarctic Mountains, Mid-Holocene outlet glacier thinning and retreat occurred during a relatively stable period of air temperature and sea level after the majority of post-glacial
375 sea level rise and rising atmospheric temperatures occurred (Lambeck et al., 2014; Jones et al., 2015; Spector et al., 2017).

Glacial reconstructions using marine geological and geophysical data along the western Ross Sea focus on tracking a grounding line that represents the ice sheet as a whole (Licht et al., 1996; Domack et al., 1999; Shipp et al., 1999; McKay et al., 2008; Anderson et al., 2014). However, there is increasing evidence that palaeo-ice streams and TAM outlet glaciers decoupled from the larger ice sheet occupying the Ross Embayment during deglaciation (Halberstadt et al., 2016; Lee et al., 2017). As the
380 grounding line retreated southward, past TAM outlet glaciers, local subglacial topography is expected to have exerted a significant control on local glacier thinning and retreat rates (Jones et al., 2015). Marine geophysical and geological data reveal a large grounding zone wedge (GZW) near Coulman Island, marking the probable LGM grounding line limit of ice in the Ross Sea (Shipp et al., 1999). Based on marine sedimentary analysis and radiocarbon age dating, the timing of retreat from the Coulman Island GZW initiated at \sim 13 ka, punctuated by few short periods of staggered retreat through the deep Drygalski
385 Trough (Licht et al., 1996; Domack et al., 1999; Anderson et al., 2014; Yokoyama et al., 2016). By \sim 10 ka, ^{14}C dating of acid insoluble organic (AIO) matter from sediment cores, suggest the grounding line in the Ross Sea migrated south of the David Glacier (Licht and Andrews, 2002). However, AIO dates in the Ross Sea are known to be unreliable due to potential input of anomalously old carbon by reworking, and this 10 ka constraint is likely to represent a maximum age of this retreat (Andrews et al., 1999; Rosenheim et al., 2013). Furthermore, short pauses in onshore thinning may temporally link to short periods of
390 stability recorded by small grounding zone wedges deep in the Drygalski Trough and near Terra Nova Bay (Brancolini et al., 1995; Anderson et al., 2014; Lee, 2019).

Interpreted sub-ice shelf facies from marine sedimentary cores collected in the deepest parts of the inner Drygalski trough provide evidence of a lingering ice shelf, but anomalously old surface ^{14}C ages hinder coherent chronologies (Licht et al., 1996; Frignani et al., 1998; Domack et al., 1999; Licht and Andrews, 2002). North of Terra Nova Bay, meteoric ^{10}Be and compound specific radiocarbon ages capture the retreating calving line and onset of open marine conditions by 8 ka ((Yokoyama et al., 2016). This timing is consistent with the raised beach chronology of Baroni and Hall (2004), which marks the local onset of coastal open marine conditions no later than 8 ka.

In summary, evidence from offshore David Glacier indicates that retreat of grounded ice through the Drygalski Trough and the formation of open marine conditions similar to today occurred immediately prior to the dynamic thinning of David Glacier recorded in this study. Together with the existing retreat chronology outlined above, our onshore surface exposure data records the final stages of glacial thinning and retreat along the David Glacier and wider Terra Nova Bay area.

5.2 Coastal thinning and impacts on local oceanography

Using continental-scale ice sheet model reconstructions and available geological data as a guide, the glacier thinning profile at Hughes Bluff likely only captures the final 200 metres of the approximately 400+ metre thinning since the LGM (Fig. S2). 405 In total, marine geological evidence, ice modelling and new results in this study suggest that at the LGM, the expanded David glacier had a surface profile above the level of Mt Kring and Hughes Bluff, and a grounding line that was pinned on the David Fiord bathymetric sill. The subsequent modelled retreat to near modern configuration reproduces both the magnitude and rate of onshore thinning derived from surface exposure data.

The new geological reconstruction of ice-surface elevation changes at Hughes Bluff shows a rapid lowering of the David 410 Glacier at 6.5 ka and a period of slow thinning from \sim 6-4 ka. Minimal ice surface lowering since \sim 6 ka likely records the stability of the grounding line within the David Fjord near the modern configuration, which suggests that the Drygalski Ice Tongue has been stable since \sim 6 ka. Orombelli et al. (1990) and Baroni and Hall (2004) mapped a series of raised beaches along 415 the Terra Nova Bay coastline that mark beach depositional processes in an open ocean setting (e.g. no grounded ice) initiating at 7.2 ka. A stable, thinned and retreated David Glacier since \sim 6 ka is broadly consistent with a raised beach chronology along the Terra Nova Bay coastline and suggests a long-term role for Drygalski Ice Tongue in sustaining the Terra Nova Bay polynya as interpreted from modern and paleo-oceanographic observations (Baroni and Hall, 2004; Stevens et al., 2017; Mezgec et al., 2017).

5.3 Interior ice sheet thinning

Our modelling demonstrates that glacier thinning at Mt. Kring is sensitive to grounding line migration during ice retreat from 420 the outer to the inner continental shelf. Mt. Kring is part of a broad bedrock platform along the northern flank of the major glacial trough dissecting the TAM (Fig. S1). The platform is comprised of three high elevation outcrops protruding \sim 200 metres above the local ice surface, with Mt. Kring nearest to the zone of streaming ice (e.g. surface velocities >100 m/yr). Geophysical characterisation of the northern TAM suggests the presence of individual tectonic blocks bounded by faults which likely serve as zones of relatively weak rock strength allowing preferential ice flow and glacial erosion (Salvini and Storti,

425 1999; Dubbini et al., 2010). In West Antarctica, dynamic thinning of the inland ice sheet has been linked to underlying tectonic controls (Bingham et al., 2012). At David Glacier, similar tectonic controls may have conditioned the spatial pattern of dynamic thinning during the Holocene.

Along the upper reaches of the David Fjord, there are no outcrops in the zone of highest surface velocity (>100 m/yr). The closest outcrop to fast-flowing ice, Mt. Kring, lies ~40 km from the modelled flowline. Modern surface velocities near 430 Mt. Kring are ~15% of the surface velocities at the projected flowline position (Rignot et al., 2011). On modern ice sheets experiencing dynamic thinning, satellite derived thinning estimates are largest in the centre of the ice streams or outlet glaciers, and become progressively smaller at lower velocity sites further from the central flowline. For example, the central parts of 435 Greenland's outlet glaciers are currently thinning at rates of ~0.84 m/yr, while marginal areas with slower ice velocities are thinning at 0.12 m/yr (Pritchard et al., 2009). Therefore, it is likely that the Mt. Kring site likely reflects ice stream marginal thinning (maximum of 0.17 m/yr, derived from surface exposure data) rather than the larger thinning rate that was experienced in the centre of an ice stream (modelled maximum 0.3 m/yr). Taken together, the Hughes Bluff and Mt. Kring chronologies suggest that ~2 kyr of dynamic thinning occurred at David Glacier, and that this thinning propagated significantly into the ice sheet interior.

5.4 Controls on thinning and grounding line migration

440 Overall, the style of modelled grounding line retreat appears to be controlled by the Marine Ice Sheet Instability (MISI), a positive feedback where grounding line retreat into subglacial basins leads to progressively enhanced ice discharge and ice sheet thinning (Weertman et al., 1974; Mercer, 1978; Schoof, 2007). The topographic profile of the western Ross Sea is dominated by the deep and landward sloping Drygalski Trough and our modelling experiments show that the grounding line 445 stabilises on a bathymetric sill at the mouth of the David Fjord. Experiments designed to simulate glacier-ice sheet decoupling show that once independent, the David Glacier grounding line rapidly retreats through the Drygalski Trough to a temporary stable position near the TAM coastline.

This study provides insights into the processes that occurred as a large grounded section of an ice sheet retreated into discrete outlet glaciers. Previous descriptions of this retreat have focused on grounded ice in the Ross Sea as a whole (Licht et al., 1996; Shipp et al., 1999; Domack et al., 1999; McKay et al., 2008; Anderson et al., 2014). However, at the scale of David Glacier, 450 retreat was likely influenced by local processes including interactions with adjacent glaciers and other ice bodies. For example, a recent ice sheet retreat reconstruction of Halberstadt et al. (2016) suggests that stable ice lingered on higher elevation banks as ice retreated in adjacent, large bathymetric troughs. Such lingering ice likely impacted lateral buttressing on David Glacier during retreat. Therefore, thinning and retreat histories of grounded ice resting on bank tops may influence ice stream lateral buttressing.

455 Knowledge of this complex lingering ice history is poorly constrained as the majority of research has focused on trough axes (Anderson et al., 2014; Halberstadt et al., 2016). Analysis of marine sediments suggests from such troughs indicate that a 'calving bay' environment formed during grounding line retreat (Domack et al., 1999, 2003; Leventer et al., 2006; Mackintosh et al., 2014). In this scenario, retreat is rapid along the trough axis while lingering ice remains along the lateral margins of

the ice stream/glacier. In addition to sedimentary evidence, the abundant large iceberg keelmarks seaward of the Coulman
460 Island GZW and smaller keelmarks within Terra Nova Bay provide evidence for a calving bay during deglaciation. Short-term
grounding line stability of the expanded David Glacier may have been facilitated by complex interaction with other outlet
glaciers (Reeves and Priestley glaciers together forming proto-Nansen Ice Sheet/Shelf) of Terra Nova Bay and/or grounded ice
lingering on the banks surrounding the Drygalski Trough.

The modelled grounding line initially retreats to a location where a large GZW has been documented by Lee (2019), possibly
465 providing an explanation for why a large GZW was deposited in this location. A lack of modelled grounding line stability at other, smaller GZWs suggests that the grounding-line may only have experienced very short stable periods in these locations. Further, in the case of the much smaller ‘GZWs’ observed in the deepest portion of the Drygalski Trough, the morphology may reflect a point source versus a line or zone source associated with more classically defined sheet-like GZWs. Regardless, the small mounds in the trough axis are likely to reflect short-lived stable positions during overall grounding line retreat.

470 Generally, once initiated, the modelled David Glacier retreats rapidly to a stable grounding line position in ~500 yrs, pausing at a prominent sill at the mouth of David Fjord for up to 5 kyr before subsequent grounding line migration led to its modern configuration. This simulated two-phase grounding line retreat compares well with our onshore reconstructions at Mt. Kring and Hughes Bluff, both in terms of timing and rates of past glacier thinning. Models forced by moderate sub-ice-shelf melt rates and lateral buttressing reduction, fit best with onshore geologic constraints.

475 Figure 12 synthesise the results of the terrestrial thinning chronology, modelled glacier flowline behaviour and the existing regional marine retreat chronologies. This synthesis suggests that beginning at 7.5 kyr, with the grounding line pinned to the sill at the mouth of the David Fjord, the David Glacier and proto-Nansen Ice Shelf decouple and widespread onshore thinning is initiated. Between 6-5.5 kyr, the grounding line retreats to near its modern position, thinning slows significantly and open marine conditions prevail regionally.

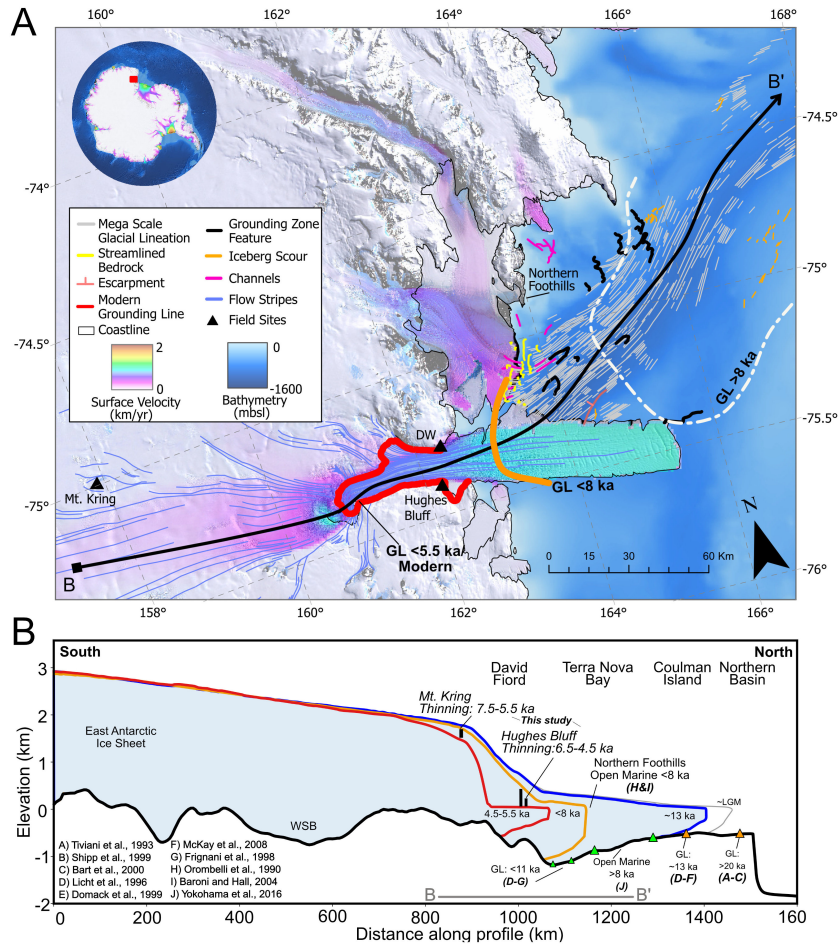


Figure 12. A) Map of Holocene thinning and retreat model for David Glacier, Terra Nova Bay. Synthesis map focused on two phase retreat between 11 ka and 5.5 ka, including geographic and geomorphic features mentioned in text. Surface velocity of (Rignot et al., 2011) and LIMA satellite data of (Bindschadler et al., 2008). Inset with red box for main extent shows bathymetry of (Arndt et al., 2013) and surface velocity of (Rignot et al., 2011). B) Synthesis profile focused on two phase retreat between 11 ka and 5.5 ka. Grounding zone features: well constrained (orange triangles), poorly constrained (green triangles). GL=Grounding line

480 6 Conclusions

Chronologies from the David Glacier reveal a period of glacier thinning along a large swath of the drainage basin during the Mid-Holocene (~ 6.5 ka). The reconstructed thinning style between two sites separated by ~ 130 km, reveals a dynamic thinning event that endured for two millennia. This chronology is synchronous with local, regional and continental scale geological records of ice sheet behaviour yet is not fully captured in continental scale ice sheet models. Our flowline modelling results suggest that thinning and grounding-line retreat was driven by increased sub-ice shelf melt rates and decreased ice stream lateral

butressing, and that the combination of these two processes produces a powerful forcing that reduces the individual forcing thresholds required to initiate retreat. Modelled episodes of grounding line retreat correlate well with periods of onshore thinning, constrained by our high-resolution surface exposure ages. Data-model mismatches highlight enduring questions related to the relative role of local topographic pinning points and glacier-ice sheet decoupling on the nature of dynamic thinning, both
490 observed and modelled.

Through careful collection of glacial deposits from numerous sites along the David Glacier, we have closed a spatial and temporal gap in the rapidly expanding onshore glacial geologic knowledge bank. Our data constrain one of the largest outlet glaciers in the world which carries regional significance for Victoria Land and the western Ross Sea, as well as offering clues about processes currently underway in rapidly changing sectors of Antarctica and Greenland. **While we acknowledge the data and modelling presented in this work may not apply to other settings, we hope that our study may serve as a template for future work aiming to extend the observations of ice sheet change beyond the last ~40 years of satellite data.**
495

Code availability. Modelling code

The code used for flowline modelling is available by request from the corresponding author.

Data availability. Geochemical data and exposure ages

500 Field, lab, analytical and exposure age data are available on ICE-D online database (antarctica.ICE-D.org) and in supplementary tables 2-6

Sample availability. Samples collected during the 2016/17 austral summer are curated at Te Herenga Waka - Victoria University of Wellington and are available from the corresponding author. Samples collected prior to 2016/17 austral summer are curated at the University of Pisa.

505 *Author contributions.* JS contributed to project design, field work planning and implementation, sample analysis, modelling and preparation of manuscript. AM contributed to original project design, field work, modelling and manuscript preparation. KN contributed to original project design, sample analysis and manuscript preparation. RW contributed to field and lab work. CB and MCS led previous regional field work, contributed data and helped prepare manuscript. SC contributed to field and lab work. SJ led modelling work and contributed to preparation of manuscript. RSJ contributed to project design and modelling work. GB contributed to project design and BGC related lab work. PS
510 contributed to Data-Model Comparison (DMC) work. JL contributed unpublished bathymetry data and regional marine geologic observations. YBS contributed to regional synthesis discussion. TW, LD, MI, FS, SIO, MC conducted AMS analyses at respective laboratories. LV

contributed through preparation of SfMP models, modelling and manuscript preparation. DL contributed to DMC work. RM contributed to regional marine geology synthesis.

Competing interests. The authors would like to declare that no competing interests are present

515 *Acknowledgements.* We would like to acknowledge NZARI (Grant 2017-1-3) for funding field work, AMS analyses and research visit to BGC. Support for a research visit to Durham University was provided by the Antarctic Science Bursary. We'd like to thank our trusty mountaineer Bia Boucinhas and pilot Mark Hayes for safe passage during field work. Logistical support for field and lab work was expertly provided by Antarctica New Zealand, Italian National Antarctic Programme (PNRA), Korean Polar Research Institute (KOPRI), Southern Lakes helicopters, Kenn Borek Air, Antarctic Research Centre, School of Geography, Earth and Environmental Studies, and Te Herenga 520 Waka - Victoria University of Wellington. We extend a great deal of gratitude for the many experienced researchers in the David Glacier area for providing field photos from past expeditions.

References

Anderson, B. M., Hindmarsh, R. C., and Lawson, W. J.: A modelling study of the response of Hatherton Glacier to Ross Ice Sheet grounding line retreat, *Global and Planetary Change*, 42, 143–153, <https://doi.org/10.1016/j.gloplacha.2003.11.006>, 2004.

525 Anderson, J. B., Conway, H., Bart, P. J., Witus, A. E., Greenwood, S. L., McKay, R. M., Hall, B. L., Ackert, R. P., Licht, K., Jakobsson, M., and Stone, J. O.: Ross Sea paleo-ice sheet drainage and deglacial history during and since the LGM, *Quaternary Science Reviews*, 100, 31–54, <https://doi.org/10.1016/j.quascirev.2013.08.020>, 2014.

Andrews, J. T., Domack, E. W., Cunningham, W. L., Leventer, A., Licht, K. J., Jull, A. J. T., DeMaster, D. J., and Jennings, A. E.: Problems and Possible Solutions Concerning Radiocarbon Dating of Surface Marine Sediments, Ross Sea, Antarctica, *Quaternary Research*, 52, 530 206–216, <https://doi.org/10.1006/qres.1999.2047>, 1999.

Argus, D. F., Peltier, W. R., Drummond, R., and Moore, A. W.: The Antarctica component of postglacial rebound model ICE-6G_C (VM5a) based on GPS positioning, exposure age dating of ice thicknesses, and relative sea level histories, *Geophysical Journal International*, 198, 535 537–563, <https://doi.org/10.1093/gji/ggu140>, 2014.

Arndt, J. E., Schenke, H. W., Jakobsson, M., Nitsche, F. O., Buys, G., Goleby, B., Rebesco, M., Bohoyo, F., Hong, J., Black, J., Greku, R., Udintsev, G., Barrios, F., Reynoso-Peralta, W., Taisei, M., and Wigley, R.: The International Bathymetric Chart of the Southern Ocean (IBCSO) Version 1.0-A new bathymetric compilation covering circum-Antarctic waters, *Geophysical Research Letters*, 40, 3111–3117, <https://doi.org/10.1002/grl.50413>, 2013.

535 Arthern, R. J., Winebrenner, D. P., and Vaughan, D. G.: Antarctic snow accumulation mapped using polarization of 4.3-cm wavelength microwave emission, *Journal of Geophysical Research Atmospheres*, 111, D06 107, <https://doi.org/10.1029/2004JD005667>, 2006.

540 Assmann, K. M., Darelius, E., Wählén, A. K., Kim, T. W., and Lee, S. H.: Warm Circumpolar Deep Water at the western Getz Ice Shelf Front, Antarctica, *Geophysical Research Letters*, <https://doi.org/10.1029/2018GL081354>, <http://doi.wiley.com/10.1029/2018GL081354>, 2019.

Atkins, C. B.: Geomorphological evidence of cold-based glacier activity in South Victoria Land, Antarctica, *Geological Society, London, Special Publications*, 381, 299–318, <https://doi.org/10.1144/SP381.18>, 2013.

545 Balco, G.: Contributions and unrealized potential contributions of cosmogenic-nuclide exposure dating to glacier chronology, 1990–2010, *Quaternary Science Reviews*, 30, 3–27, <https://doi.org/10.1016/j.quascirev.2010.11.003>, 2011.

Balco, G.: Technical note: A prototype transparent-middle-layer data management and analysis infrastructure for cosmogenic-nuclide exposure dating, *Geochronology*, 2, 169–175, <https://doi.org/10.5194/gchron-2-169-2020>, 2020.

550 Balco, G., Stone, J. O., Lifton, N. A., and Dunai, T. J.: A complete and easily accessible means of calculating surface exposure ages or erosion rates from ^{10}Be and ^{26}Al measurements, *Quaternary Geochronology*, 3, 174–195, <https://doi.org/10.1016/J.QUAGEO.2007.12.001>, <https://www.sciencedirect.com/science/article/pii/S1871101407000647>, 2008.

Balter-Kennedy, A., Bromley, G., Balco, G., Thomas, H., and Jackson, M. S.: A 14.5-million-year record of East Antarctic Ice Sheet fluctuations from the central Transantarctic Mountains, constrained with cosmogenic ^{3}He , ^{10}Be , ^{21}Ne , and ^{26}Al , *The Cryosphere*, 14, 2647–2672, <https://doi.org/10.5194/tc-14-2647-2020>, <https://tc.copernicus.org/articles/14/2647/2020/>, 2020.

Baroni, C. and Hall, B. L.: A new Holocene relative sea-level curve for Terra Nova Bay, Victoria Land, Antarctica, *Journal of Quaternary Science*, 19, 377–396, <https://doi.org/10.1002/jqs.825>, 2004.

555 Baroni, C., Frezzotti, M., Salvatore, M. C., Meneghel, M., Tabacco, I. E., Vittuari, L., Bondesan, A., Biasini, A., Cimbelli, A., and Orombelli, G.: Antarctic geomorphological and glaciological 1 : 250 000 map series: Mount Murchison quadrangle, northern Victoria Land. Explanatory notes, *Annals of Glaciology*, 39, 256–264, <https://doi.org/10.3189/172756404781814131>, 2004.

Bentley, M., Hein, A., Sugden, D., Whitehouse, P., Shanks, R., Xu, S., and Freeman, S.: Deglacial history of the Pensacola Mountains, 560 Antarctica from glacial geomorphology and cosmogenic nuclide surface exposure dating, *Quaternary Science Reviews*, 158, 58–76, <https://doi.org/10.1016/j.quascirev.2016.09.028>, 2017.

Bentley, M. J., O Cofaigh, C., Anderson, J. B., Conway, H., Davies, B., Graham, A. G., Hillenbrand, C.-D., Hodgson, D. A., Jamieson, 565 S. S., Larter, R. D., Mackintosh, A., Smith, J. A., Verleyen, E., Ackert, R. P., Bart, P. J., Berg, S., Brunstein, D., Canals, M., Colhoun, E. A., Crosta, X., Dickens, W. A., Domack, E., Dowdeswell, J. A., Dunbar, R., Ehrmann, W., Evans, J., Favier, V., Fink, D., Fogwill, C. J., Glasser, N. F., Gohl, K., Golledge, N. R., Goodwin, I., Gore, D. B., Greenwood, S. L., Hall, B. L., Hall, K., Hedding, D. W., Hein, A. S., Hocking, E. P., Jakobsson, M., Johnson, J. S., Jomelli, V., Jones, R. S., Klages, J. P., Kristoffersen, Y., Kuhn, G., Leventer, A., Licht, K., Lilly, K., Lindow, J., Livingstone, S. J., Massé, G., McGlone, M. S., McKay, R. M., Melles, M., Miura, H., Mulvaney, R., Nel, W., Nitsche, F. O., O'Brien, P. E., Post, A. L., Roberts, S. J., Saunders, K. M., Selkirk, P. M., Simms, A. R., Spiegel, C., Stolldorf, T. D., Sugden, D. E., van der Putten, N., van Ommen, T., Verfaillie, D., Vyverman, W., Wagner, B., White, D. A., Witus, A. E., and Zwart, D.: 570 A community-based geological reconstruction of Antarctic Ice Sheet deglaciation since the Last Glacial Maximum, *Quaternary Science Reviews*, 100, 1–9, <https://doi.org/10.1016/j.quascirev.2014.06.025>, 2014.

Bindschadler, R., Vornberger, P., Fleming, A., Fox, A., Mullins, J., Binnie, D., Paulsen, S., Granneman, B., and Gorodetsky, D.: The Landsat 575 Image Mosaic of Antarctica, *Remote Sensing of Environment*, 112, 4214–4226, <https://doi.org/10.1016/j.rse.2008.07.006>, 2008.

Bingham, R. G., Ferraccioli, F., King, E. C., Larter, R. D., Pritchard, H. D., Smith, A. M., and Vaughan, D. G.: Inland thinning of West 580 Antarctic Ice Sheet steered along subglacial rifts, *Nature*, 487, 468–471, <https://doi.org/10.1038/nature11292>, <http://www.nature.com/articles/nature11292>, 2012.

Blard, P.-H., Balco, G., Burnard, P., Farley, K., Fenton, C., Friedrich, R., Jull, A., Niedermann, S., Pik, R., Schaefer, J., Scott, E., Shuster, D., 585 Stuart, F., Stute, M., Tibari, B., Winckler, G., and Zimmermann, L.: An inter-laboratory comparison of cosmogenic ^{3}He and radiogenic ^{4}He in the CRONUS-P pyroxene standard, *Quaternary Geochronology*, 26, 11–19, <https://doi.org/10.1016/j.quageo.2014.08.004>, 2015.

Bockheim, J. G., Wilson, S. C., Denton, G. H., Andersen, B. G. B. G., and Stuiver, M.: Late Quaternary ice-surface fluctuations of Hatherton 590 Glacier, Transantarctic Mountains, *Quaternary Research*, 31, 229–254, [https://doi.org/10.1016/0033-5894\(89\)90007-0](https://doi.org/10.1016/0033-5894(89)90007-0), 1989.

Brancolini, G., Cooper, A. K., and Coren, F.: Seismic Facies and Glacial History in the Western Ross Sea (Antarctica), *Geology and Seismic 595 Stratigraphy of the Antarctic Margin*, AGU Antarctic Research Series, 68, 209–233, 1995.

Bromley, G. R., Winckler, G., Schaefer, J. M., Kaplan, M. R., Licht, K. J., and Hall, B. L.: Pyroxene separation by HF leaching and its 600 impact on helium surface-exposure dating, *Quaternary Geochronology*, 23, 1–8, <https://doi.org/10.1016/J.QUAGEO.2014.04.003>, <http://www.sciencedirect.com/science/article/pii/S1871101414000351>, 2014.

Buiron, D., Chappellaz, J., Stenni, B., Frezzotti, M., Baumgartner, M., Capron, E., Landais, A., Lemieux-Dudon, B., Masson-Delmotte, V., 605 Montagnat, M., Parrenin, F., and Schilt, A.: TALDICE-1 age scale of the Talos Dome deep ice core, East Antarctica, *Climate of the Past*, 7, 1–16, <https://doi.org/10.5194/cp-7-1-2011>, 2011.

Cavitte, M. G. P., Parrenin, F., Ritz, C., Young, D. A., Van Liefferinge, B., Blankenship, D. D., Frezzotti, M., and Roberts, J. L.: Accumulation 610 patterns around Dome C, East Antarctica, in the last 73 kyr, *The Cryosphere*, 12, 1401–1414, <https://doi.org/10.5194/tc-12-1401-2018>, <http://www.the-cryosphere.net/12/1401/2018/>, 2018.

Clason, C. C., Greenwood, S. L., Selmes, N., Lea, J. M., Jamieson, S. S. R., Nick, F. M., and Holmlund, P.: Controls on the 615 early Holocene collapse of the Bothnian Sea Ice Stream, *Journal of Geophysical Research: Earth Surface*, 121, 2494–2513, <https://doi.org/10.1002/2016JF004050>, 2016.

Denton, G. H., Bockheim, J. G., Wilson, S. C., Leide, J. E., and Andersen, B. G.: Late Quaternary Ice-Surface Fluctuations of Beardmore Glacier, Transantarctic Mountains, *Quaternary Research*, 31, 183–209, [https://doi.org/10.1016/0033-5894\(89\)90005-7](https://doi.org/10.1016/0033-5894(89)90005-7), 1989.

Di Nicola, L., Strasky, S., Schlüchter, C., Salvatore, M. C., Akçar, N., Kubik, P. W., Christl, M., Kasper, H. U., Wieler, R., and Baroni, C.: Multiple cosmogenic nuclides document complex Pleistocene exposure history of glacial drifts in Terra Nova Bay (northern Victoria Land, Antarctica), *Quaternary Research*, 71, 83–92, <https://doi.org/10.1016/j.yqres.2008.07.004>, 2009.

600 Di Nicola, L., Baroni, C., Strasky, S., Salvatore, M. C., Schlüchter, C., Akçar, N., Kubik, P. W., and Wieler, R.: Multiple cosmogenic nuclides document the stability of the East Antarctic Ice Sheet in northern Victoria Land since the Late Miocene (5–7 Ma), *Quaternary Science Reviews*, 57, 85–94, <https://doi.org/10.1016/j.quascirev.2012.09.026>, 2012.

Domack, E., Leventer, A., Dunbar, R., Brachfeld, S., Manley, P., and McClenen, C.: Calving Bay Reentrants During the Late Pleistocene to Holocene Retreat of the Antarctic Ice Sheet: Sedimentologic and Geomorphologic Evidence, AGU FM, 2003, PP32D-07, <https://ui.adsabs.harvard.edu/abs/2003AGUFMPP32D..07D/abstract>, 2003.

605 Domack, E. W., Jacobson, E. A., Shipp, S., and Anderson, J. B.: Late Pleistocene–Holocene retreat of the West Antarctic Ice-Sheet system in the Ross Sea: Part 2—Sedimentologic and stratigraphic signature, *Geological Society of America Bulletin*, 111, 1517, [https://doi.org/10.1130/0016-7606\(1999\)111<1517:LPHROT>2.3.CO;2](https://doi.org/10.1130/0016-7606(1999)111<1517:LPHROT>2.3.CO;2), <https://pubs.geoscienceworld.org/gsabulletin/article/111/10/1517-1536/183433>, 1999.

Dowdeswell, J. A., Cofaigh, C. O., and Pudsey, C. J.: Thickness and extent of the subglacial till layer beneath an Antarctic paleo-ice stream, *Geology*, 32, 13, <https://doi.org/10.1130/G19864.1>, <https://pubs.geoscienceworld.org/geology/article/32/1/13-16/129195>, 2004.

Dowdeswell, J. A., Canals, M., Jakobsson, M., Todd, B. J., Dowdeswell, E. K., and Hogan, K. A.: Introduction: an Atlas of Submarine Glacial Landforms, *Geological Society, London, Memoirs*, 46, 3–14, <https://doi.org/10.1144/M46.171>, 2016.

610 Dubbini, M., Cianfarra, P., Casula, G., Capra, A., and Salvini, F.: Active tectonics in northern Victoria Land (Antarctica) inferred from the integration of GPS data and geologic setting, *Journal of Geophysical Research*, 115, B12 421, <https://doi.org/10.1029/2009JB007123>, 2010.

Dutrieux, P., De Rydt, J., Jenkins, A., Holland, P. R., Ha, H. K., Lee, S. H., Steig, E. J., Ding, Q., Abrahamsen, E. P., and Schröder, M.: Strong sensitivity of Pine Island ice-shelf melting to climatic variability., *Science (New York, N.Y.)*, 343, 174–8, <https://doi.org/10.1126/science.1244341>, 2014.

615 Enderlin, E. M., Howat, I. M., and Vieli, A.: High sensitivity of tidewater outlet glacier dynamics to shape, *The Cryosphere*, 7, 1007–1015, <https://doi.org/10.5194/tc-7-1007-2013>, <https://www.the-cryosphere.net/7/1007/2013/>, 2013.

Fretwell, P., Pritchard, H. D., Vaughan, D. G., Bamber, J. L., Barrand, N. E., Bell, R., Bianchi, C., Bingham, R. G., Blankenship, D. D., Casassa, G., Catania, G., Callens, D., Conway, H., Cook, A. J., Corr, H. F. J., Damaske, D., Damm, V., Ferraccioli, F., Forsberg, R., Fujita, S., Gim, Y., Gogineni, P., Griggs, J. A., Hindmarsh, R. C. A., Holmlund, P., Holt, J. W., Jacobel, R. W., Jenkins, A., Jokat, W., Jordan, T., King, E. C., Kohler, J., Krabill, W., Riger-Kusk, M., Langley, K. A., Leitchenkov, G., Leuschen, C., Luyendyk, B. P., Matsuoka, K., Mouginot, J., Nitsche, F. O., Nogi, Y., Nost, O. A., Popov, S. V., Rignot, E., Rippin, D. M., Rivera, A., Roberts, J., Ross, N., Siegert, M. J., Smith, A. M., Steinhage, D., Studinger, M., Sun, B., Tinto, B. K., Welch, B. C., Wilson, D., Young, D. A., Xiangbin, C., and Zirizzotti, A.: Bedmap2: Improved ice bed, surface and thickness datasets for Antarctica, *The Cryosphere*, 7, 375–393, <https://doi.org/10.5194/tc-7-375-2013>, 2013.

620 Frezzotti, M., Pourchet, M., Flora, O., Gandolfi, S., Gay, M., Urbini, S., Vincent, C., Becagli, S., Gragnani, R., Proposito, M., Severi, M., Traversi, R., Udisti, R., and Fily, M.: Spatial and temporal variability of snow accumulation in East Antarctica from traverse data, *Journal of Glaciology*, 51, 2005.

Frignani, M., Giglio, F., Langone, L., Ravaioli, M., and Mangini, A.: Late Pleistocene-Holocene sedimentary fluxes of organic carbon and
635 biogenic silica in the northwestern Ross Sea, Antarctica, *Annals of Glaciology*, 27, 697–703, <https://doi.org/10.3189/1998AoG27-1-697-703>, https://www.cambridge.org/core/product/identifier/S0260305500018280/type/journal_article, 1998.

Giorgetti, G. and Baroni, C.: High-resolution analysis of silica and sulphate-rich rock varnishes from Victoria Land (Antarctica), *European Journal of Mineralogy*, 19, 381–389, <https://doi.org/10.1127/0935-1221/2007/0019-1725>, 2007.

Goehring, B. M., Balco, G., Todd, C., Moening-Swanson, I., and Nichols, K.: Late-glacial grounding line retreat in the north-
640 ern Ross Sea, Antarctica, *Geology*, <https://doi.org/10.1130/G45413.1>, <https://pubs.geoscienceworld.org/gsa/geology/article/568835/Lateglacial-grounding-line-retreat-in-the-northern>, 2019.

Halberstadt, A. R. W., Simkins, L. M., Greenwood, S. L., and Anderson, J. B.: Past ice-sheet behaviour: retreat scenarios and changing
controls in the Ross Sea, Antarctica, *The Cryosphere*, 10, 1003–1020, <https://doi.org/10.5194/tc-10-1003-2016>, 2016.

Hall, B. L.: Holocene glacial history of Antarctica and the sub-Antarctic islands, *Quaternary Science Reviews*, 28, 2213–2230,
645 <https://doi.org/10.1016/j.quascirev.2009.06.011>, 2009.

Howat, I. M., Porter, C., Smith, B. E., Noh, M.-J., and Morin, P.: The Reference Elevation Model of Antarctica, *The Cryosphere*, 13, 665–674,
<https://doi.org/10.5194/tc-13-665-2019>, <https://www.the-cryosphere.net/13/665/2019/>, 2019.

IMBIE, T.: Mass balance of the Antarctic Ice Sheet from 1992 to 2017, *Nature*, 558, 219–222, <https://doi.org/10.1038/s41586-018-0179-y>,
<http://www.nature.com/articles/s41586-018-0179-y>, 2018.

650 IPCC: Climate Change 2013: The Physical Science Basis. Contribution of Working Group I to the Fifth Assessment Report of the Intergovernmental Panel on Climate Change, Tech. rep., IPCC, 2013.

Jamieson, S. S. R., Vieli, A., Livingstone, S. J., Cofaigh, C. O., Stokes, C., Hillenbrand, C.-D., and Dowdeswell, J. A.: Ice-stream stability
on a reverse bed slope, *Nature Geoscience*, 5, 799–802, <https://doi.org/10.1038/NGEO1600>, 2012.

Jamieson, S. S. R., Vieli, A., Cofaigh, C. O., Stokes, C. R., Livingstone, S. J., and Hillenbrand, C.-D.: Understanding controls on rapid
655 ice-stream retreat during the last deglaciation of Marguerite Bay, Antarctica, using a numerical model, *Journal of Geophysical Research: Earth Surface*, 119, 247–263, <https://doi.org/10.1002/2013JF002934>, 2014.

Johnson, J. S., Hillenbrand, C.-D., Smellie, J. L., and Rocchi, S.: The last deglaciation of Cape Adare, northern Victoria
Land, *Antarctic Science*, 20, 581, <https://doi.org/10.1017/S0954102008001417>, http://www.journals.cambridge.org/abstract_S0954102008001417, 2008.

660 Johnson, J. S., Bentley, M. J., Smith, J. A., Finkel, R. C., Rood, D. H., Gohl, K., Balco, G., Larter, R. D., and Schaefer, J. M.: Rapid Thinning
of Pine Island Glacier in the Early Holocene, *Science*, 343, 2014.

Johnson, J. S., Nichols, K. A., Goehring, B. M., Balco, G., and Schaefer, J. M.: Abrupt mid-Holocene ice loss in the western Weddell
Sea Embayment of Antarctica, *Earth and Planetary Science Letters*, 518, 127–135, <https://doi.org/10.1016/J.EPSL.2019.05.002>, <http://www.sciencedirect.com/science/article/pii/S0012821X19302638#ec0020>, 2019.

665 Jones, R., Small, D., Cahill, N., Bentley, M., and Whitehouse, P.: iceTEA: Tools for plotting and analysing cosmogenic-nuclide surface-
exposure data from former ice margins, *Quaternary Geochronology*, <https://doi.org/10.1016/J.QUAGEO.2019.01.001>, <https://www.sciencedirect.com/science/article/pii/S1871101418301110>, 2019.

Jones, R. S., Mackintosh, A. N., Norton, K. P., Golledge, N. R., Fogwill, C. J., Kubik, P. W., Christl, M., and Greenwood, S. L.:
Rapid Holocene thinning of an East Antarctic outlet glacier driven by marine ice sheet instability, *Nature Communications*, 6,
670 <https://doi.org/10.1038/ncomms9910>, 2015.

Joughin, I., Bamber, J. L., Scambos, T., Tulaczyk, S., Fahnestock, M., and MacAyeal, D. R.: Integrating satellite observations with modelling: basal shear stress of the Filcher-Ronne ice streams, Antarctica, *Philosophical Transactions of the Royal Society A: Mathematical, Physical and Engineering Sciences*, 364, 1795–1814, <https://doi.org/10.1098/rsta.2006.1799>, <https://royalsocietypublishing.org/doi/10.1098/rsta.2006.1799>, 2006.

675 Joy, K., Fink, D., Storey, B., and Atkins, C.: A 2 million year glacial chronology of the Hatherton Glacier, Antarctica and implications for the size of the East Antarctic Ice Sheet at the Last Glacial Maximum, *Quaternary Science Reviews*, 83, 46–57, <https://doi.org/10.1016/j.quascirev.2013.10.028>, 2014.

King, M. A., Bingham, R. J., Moore, P., Whitehouse, P. L., Bentley, M. J., and Milne, G. A.: Lower satellite-gravimetry estimates of Antarctic sea-level contribution, *Nature*, 491, 586–589, <https://doi.org/10.1038/nature11621>, 2012.

680 Kingslake, J., Scherer, R. P., Albrecht, T., Coenen, J., Powell, R. D., Reese, R., Stansell, N. D., Tulaczyk, S., Wearing, M. G., and Whitehouse, P. L.: Extensive retreat and re-advance of the West Antarctic Ice Sheet during the Holocene, *Nature*, 558, 430–434, <https://doi.org/10.1038/s41586-018-0208-x>, <http://www.nature.com/articles/s41586-018-0208-x>, 2018.

Lambeck, K., Rouby, H., Purcell, A., Sun, Y., and Sambridge, M.: Sea level and global ice volumes from the Last Glacial Maximum to the Holocene., *Proceedings of the National Academy of Sciences of the United States of America*, 111, 15 296–303, <https://doi.org/10.1073/pnas.1411762111>, 2014.

685 Lee, J. I.: Onshore to Offshore glacial reconstruction of Terra Nova Bay, Western Ross Sea, in: XIII International Symposium on Antarctic Earth Sciences: Workshop, KOPRI, Incheon, 2019.

Lee, J. I., McKay, R. M., Golledge, N. R., Yoon, H. I., Yoo, K.-C., Kim, H. J., and Hong, J. K.: Widespread persistence of expanded East Antarctic glaciers in the southwest Ross Sea during the last deglaciation, *Geology*, 45, 403–406, <https://doi.org/10.1130/G38715.1>, <https://pubs.geoscienceworld.org/geology/article/45/5/403-406/207900>, 2017.

690 Lenaerts, J. T. M., van den Broeke, M. R., van de Berg, W. J., van Meijgaard, E., and Kuipers Munneke, P.: A new, high-resolution surface mass balance map of Antarctica (1979–2010) based on regional atmospheric climate modeling, *Geophysical Research Letters*, 39, n/a–n/a, <https://doi.org/10.1029/2011GL050713>, <http://doi.wiley.com/10.1029/2011GL050713>, 2012.

Leventer, A., Domack, E., Dunbar, R., Pike, J., Stickley, C., Maddison, E., Brachfeld, S., Manley, P., and McClenen, C.: Marine sediment record from the East Antarctic margin reveals dynamics of ice sheet recession, *GSA Today*, 16, 4, <https://doi.org/10.1130/GSAT01612A.1>, <ftp://rock.geosociety.org/pub/GSAToday/gt0612.pdf>, 2006.

695 Licht, K. J. and Andrews, J. T.: The 14 C Record of Late Pleistocene Ice Advance and Retreat in the Central Ross Sea, Antarctica, Arctic, Antarctic, and Alpine Research, 34, 324, <https://doi.org/10.2307/1552491>, 2002.

Licht, K. J., Jennings, A. E., Andrews, J. T., and Williams, K. M.: Chronology of late Wisconsin ice retreat from the western Ross Sea, Antarctica, *Geology*, 24, 223–226, [https://doi.org/10.1130/0091-7613\(1996\)024<0223:COLWIR>2.3.CO;2](https://doi.org/10.1130/0091-7613(1996)024<0223:COLWIR>2.3.CO;2), 1996.

700 Lifton, N., Sato, T., and Dunai, T. J.: Scaling in situ cosmogenic nuclide production rates using analytical approximations to atmospheric cosmic-ray fluxes, *Earth and Planetary Science Letters*, 386, 149–160, <https://doi.org/10.1016/J.EPSL.2013.10.052>, <https://www.sciencedirect.com/science/article/pii/S0012821X13006316>, 2014.

Liu, Z., Otto-Bliesner, B. L., He, F., Brady, E. C., Tomas, R., Clark, P. U., Carlson, A. E., Lynch-Stieglitz, J., Curry, W., Brook, E., Erickson, D., Jacob, R., Kutzbach, J., and Cheng, J.: Transient simulation of last deglaciation with a new mechanism for bolling-allerod warming, *Science*, 325, 310–314, <https://doi.org/10.1126/science.1171041>, www.sciencemag.org/cgi/content/full/325/5938/306/DC1, 2009.

Livingstone, S. J., O Cofaigh, C., Stokes, C. R., Hillenbrand, C.-D., Vieli, A., and Jamieson, S. S.: Antarctic palaeo-ice streams, *Earth-Science Reviews*, 111, 90–128, <https://doi.org/10.1016/j.earscirev.2011.10.003>, 2012.

Livingstone, S. J., Stokes, C. R., Cofaigh, C., Hillenbrand, C. D., Vieli, A., Jamieson, S. S. R., Spagnolo, M., and Dowdeswell, J. A.:
710 Subglacial processes on an Antarctic ice stream bed. 1: Sediment transport and bedform genesis inferred from marine geophysical data, Journal of Glaciology, 62, 270–284, <https://doi.org/10.1017/jog.2016.18>, 2016.

Lowry, D. P., Golledge, N. R., Bertler, N. A. N., Jones, R. S., and McKay, R.: Deglacial grounding-line retreat in the Ross Embayment, Antarctica, controlled by ocean and atmosphere forcing, Science Advances, 5, <https://doi.org/10.1126/sciadv.aav8754>, <https://advances.sciencemag.org/lookup/doi/10.1126/sciadv.aav8754>, 2019.

715 Lowry, D. P., Golledge, N. R., Bertler, N. A., Jones, R. S., McKay, R., and Stutz, J.: Geologic controls on ice sheet sensitivity to deglacial climate forcing in the Ross Embayment, Antarctica, Quaternary Science Advances, 1, 100 002, <https://doi.org/10.1016/J.QSA.2020.100002>, <https://www.sciencedirect.com/science/article/pii/S2666033420300022>, 2020.

Mackintosh, A., White, D., Fink, D., Gore, D. B., Pickard, J., and Fanning, P. C.: Exposure ages from mountain dipsticks in Mac. Robertson Land, East Antarctica, indicate little change in ice-sheet thickness since the Last Glacial Maximum, Geology, 35, 551, 720 <https://doi.org/10.1130/G23503A.1>, 2007.

Mackintosh, A. N., Verleyen, E., O'Brien, P. E., White, D. A., Jones, R. S., McKay, R., Dunbar, R., Gore, D. B., Fink, D., Post, A. L., Miura, H., Leventer, A., Goodwin, I., Hodgson, D. A., Lilly, K., Crosta, X., Golledge, N. R., Wagner, B., Berg, S., van Ommen, T., Zwart, D., Roberts, S. J., Vyverman, W., and Masse, G.: Retreat history of the East Antarctic Ice Sheet since the Last Glacial Maximum, Quaternary Science Reviews, 100, 10–30, <https://doi.org/10.1016/J.QUASCIREV.2013.07.024>, <https://www.sciencedirect.com/science/article/pii/S0277379113002898>, 2014.

725 Marrero, S. M., Phillips, F. M., Borchers, B., Lifton, N., Aumer, R., and Balco, G.: Cosmogenic nuclide systematics and the CRONUS-calc program, Quaternary Geochronology, 31, 160–187, <https://doi.org/10.1016/J.QUAGEO.2015.09.005>, <https://www.sciencedirect.com/science/article/pii/S1871101415300595>, 2016.

McKay, R., Golledge, N. R., Maas, S., Naish, T., Levy, R., Dunbar, G., and Kuhn, G.: Antarctic marine ice-sheet retreat in the Ross Sea 730 during the early Holocene, Geology, 44, 7–10, <https://doi.org/10.1130/G37315.1>, 2016.

McKay, R. M., Dunbar, G. B., Naish, T. R., Barrett, P. J., Carter, L., and Harper, M.: Retreat history of the Ross Ice Sheet (Shelf) since the 735 Last Glacial Maximum from deep-basin sediment cores around Ross Island, Palaeogeography, Palaeoclimatology, Palaeoecology, 260, 245–261, <https://doi.org/10.1016/j.palaeo.2007.08.015>, 2008.

Menviel, L., Timmermann, A., Timm, O. E., and Mouchet, A.: Deconstructing the Last Glacial termination: The role of millennial and 740 orbital-scale forcings, Quaternary Science Reviews, 30, 1155–1172, <https://doi.org/10.1016/j.quascirev.2011.02.005>, 2011.

Mercer, J. H.: West Antarctic ice sheet and CO₂ greenhouse effect: a threat of disaster, Nature, 271, 321–325, <https://doi.org/10.1038/271321a0>, 1978.

745 Mezgec, K., Stenni, B., Crosta, X., Masson-Delmotte, V., Baroni, C., Braida, M., Ciardini, V., Colizza, E., Melis, R., Salvatore, M. C., Severi, M., Scarchilli, C., Traversi, R., Udisti, R., and Frezzotti, M.: Holocene sea ice variability driven by wind and polynya efficiency in the Ross Sea, Nature Communications, 8, 1–12, <https://doi.org/10.1038/s41467-017-01455-x>, 2017.

Miles, B. W. J., Stokes, C. R., Vieli, A., and Cox, N. J.: Rapid, climate-driven changes in outlet glaciers on the Pacific coast of East Antarctica, Nature, 500, 563–566, <https://doi.org/10.1038/nature12382>, 2013.

Morlighem, M., Rignot, E., Binder, T., Blankenship, D., Drews, R., Eagles, G., Eisen, O., Ferraccioli, F., Forsberg, R., Fretwell, P., and others: Deep glacial troughs and stabilizing ridges unveiled beneath the margins of the Antarctic ice sheet, Nature Geoscience, pp. 1–6, 750 2019.

Nichols, K. A., Goehring, B. M., Balco, G., Johnson, J. S., Hein, A. S., and Todd, C.: New Last Glacial Maximum ice thickness constraints for the Weddell Sea Embayment, Antarctica, *The Cryosphere*, 13, 2935–2951, <https://doi.org/10.5194/tc-13-2935-2019>, <https://www.the-cryosphere.net/13/2935/2019/>, 2019.

Nick, F. M., Vieli, A., Howat, I. M., and Joughin, I.: Large-scale changes in Greenland outlet glacier dynamics triggered at the terminus, 750 *Nature Geoscience*, 2, 110–114, <https://doi.org/10.1038/NGEO394>, 2009.

Nick, F. M., Van Der Veen, C. J., Vieli, A., and Benn, D. I.: A physically based calving model applied to marine outlet glaciers and implications for the glacier dynamics, *Journal of Glaciology*, 56, 781–794, <https://doi.org/10.3189/002214310794457344>, 2010.

Norton, K. P., von Blanckenburg, F., Schlunegger, F., Schwab, M., and Kubik, P. W.: Cosmogenic nuclide-based investigation of spatial erosion and hillslope channel coupling in the transient foreland of the Swiss Alps, *Geomorphology*, 95, 474–486, 755 <https://doi.org/10.1016/J.GEOMORPH.2007.07.013>, <https://www.sciencedirect.com/science/article/pii/S0169555X07003509>, 2008.

O Cofaigh, C., Dowdeswell, J. A., Allen, C. S., Hiemstra, J. F., Pudsey, C. J., Evans, J., and J.A. Evans, D.: Flow dynamics and till genesis associated with a marine-based Antarctic palaeo-ice stream, *Quaternary Science Reviews*, 24, 709–740, <https://doi.org/10.1016/J.QUASCIREV.2004.10.006>, <https://www.sciencedirect.com/science/article/abs/pii/S0277379104003014>, 2005.

Oberholzer, P., Baroni, C., Schaefer, J., Orombelli, G., Ochs, S. I., W., K. P., Baur, H., and Wieler, R.: Limited Pliocene/Pleistocene glaciation 760 in Deep Freeze Range, northern Victoria Land, Antarctica, derived from in situ cosmogenic nuclides, *Antarctic Science*, 15, 493–502, <https://doi.org/10.1017/S0954102003001603>, 2003.

Oberholzer, P., Baroni, C., Salvatore, M., Baur, H., and Wieler, R.: Dating late Cenozoic erosional surfaces in Victoria Land, Antarctica, with cosmogenic neon in pyroxenes, *Antarctic Science*, 20, <https://doi.org/10.1017/S095410200700079X>, 2008.

Orombelli, G., Baroni, C., and Denton, G. H.: Late Cenozoic Glacial History of the Terra Nova Bay Region, Northern Victoria Land, 765 *Antarctica, Geografia Fisica e Dinamica Quaternaria*, 13, 139–163, 1990.

Paxman, G. J., Jamieson, S. S., Hochmuth, K., Gohl, K., Bentley, M. J., Leitchenkov, G., and Ferraccioli, F.: Reconstructions of Antarctic topography since the Eocene–Oligocene boundary, *Palaeogeography, Palaeoclimatology, Palaeoecology*, 535, 109 346, <https://doi.org/10.1016/J.PALAEO.2019.109346>, <https://www.sciencedirect.com/science/article/pii/S0031018219304845>, 2019.

Pedro, J. B., Bostock, H. C., Bitz, C. M., He, F., Vandergoes, M. J., Steig, E. J., Chase, B. M., Krause, C. E., Rasmussen, S. O., 770 Markle, B. R., and Cortese, G.: The spatial extent and dynamics of the Antarctic Cold Reversal, *Nature Geoscience*, 9, 51–55, <https://doi.org/10.1038/ngeo2580>, <http://www.nature.com/articles/ngeo2580>, 2016.

Pollard, D., Chang, W., Haran, M., Applegate, P., and DeConto, R.: Large ensemble modeling of the last deglacial retreat of the West Antarctic Ice Sheet: comparison of simple and advanced statistical techniques, *Geoscientific Model Development*, 9, 1697–1723, <https://doi.org/10.5194/gmd-9-1697-2016>, <https://www.geosci-model-dev.net/9/1697/2016/>, 2016.

Pollard, D., Gomez, N., and DeConto, R. M.: Variations of the Antarctic Ice Sheet in a Coupled Ice Sheet-Earth-Sea Level Model: Sensitivity 775 to Viscoelastic Earth Properties, *Journal of Geophysical Research: Earth Surface*, 122, 2124–2138, <https://doi.org/10.1002/2017JF004371>, <http://doi.wiley.com/10.1002/2017JF004371>, 2017.

Pollard, D., Gomez, N., DeConto, R. M., and Han, H. K.: Estimating Modern Elevations of Pliocene Shorelines Using a Coupled Ice Sheet-Earth-Sea Level Model, *Journal of Geophysical Research: Earth Surface*, 123, 2279–2291, <https://doi.org/10.1029/2018JF004745>, 780 <https://onlinelibrary.wiley.com/doi/abs/10.1029/2018JF004745>, 2018.

Pritchard, H. D., Arthern, R. J., Vaughan, D. G., and Edwards, L. A.: Extensive dynamic thinning on the margins of the Greenland and Antarctic ice sheets, *Nature*, 461, 971–975, <https://doi.org/10.1038/nature08471>, <http://www.nature.com/articles/nature08471>, 2009.

Pritchard, H. D., Ligtenberg, S. R. M., Fricker, H. A., Vaughan, D. G., van den Broeke, M. R., and Padman, L.: Antarctic ice-sheet loss driven by basal melting of ice shelves, *Nature*, 484, 502–505, <https://doi.org/10.1038/nature10968>, <http://www.nature.com/articles/nature10968>, 785 2012.

Rhee, H. H., Lee, M. K., Seong, Y. B., Hong, S., Lee, J. I., Yoo, K.-C., and Yu, B. Y.: Timing of the local last glacial maximum in Terra Nova Bay, Antarctica defined by cosmogenic dating, *Quaternary Science Reviews*, 221, 105 897, <https://doi.org/10.1016/J.QUASCIREV.2019.105897>, <https://www.sciencedirect.com/science/article/pii/S0277379119303373#fig6>, 2019.

Rignot, E., Mouginot, J., and Scheuchl, B.: Ice flow of the Antarctic ice sheet., *Science* (New York, N.Y.), 333, 1427–30, 790 <https://doi.org/10.1126/science.1208336>, 2011.

Rignot, E., Mouginot, J., Scheuchl, B., Broeke, M. v. d., Wessem, M. J. v., and Morlighem, M.: Four decades of Antarctic Ice Sheet mass balance from 1979–2017, *Proceedings of the National Academy of Sciences*, 116, 1095–1103, <https://doi.org/10.1073/PNAS.1812883116>, <https://www.pnas.org/content/116/4/1095>, 2019.

Rosenheim, B. E., Santoro, J. A., Gunter, M., and Domack, E. W.: Improving Antarctic Sediment ¹⁴C Dating Using Ramped Pyrolysis: An 795 Example from the Hugo Island Trough, *Radiocarbon*, 55, 115–126, <https://doi.org/10.1017/s0033822200047846>, 2013.

Salvini, F. and Storti, F.: Cenozoic tectonic lineaments of the Terra Nova Bay region, Ross Embayment, Antarctica, *Global and Planetary Change*, 23, 129–144, [https://doi.org/10.1016/S0921-8181\(99\)00054-5](https://doi.org/10.1016/S0921-8181(99)00054-5), <https://www.sciencedirect.com/science/article/pii/S0921818199000545>, 1999.

Schoof, C.: Ice sheet grounding line dynamics: Steady states, stability, and hysteresis, *Journal of Geophysical Research: Earth Surface*, 112, 800 1–19, <https://doi.org/10.1029/2006JF000664>, 2007.

Shipp, S., Anderson, J. B., Domack, E. W., Jacobson, E. A., Shipp, S., and Anderson, J. B.: Late Pleistocene–Holocene retreat of the West Antarctic Ice-Sheet system in the Ross Sea: Part 1—Geophysical results, *GSA Bulletin*, 111, 1517–1536, [https://doi.org/10.1130/0016-7606\(1999\)111<1486:LPHROT>2.3.CO;2](https://doi.org/10.1130/0016-7606(1999)111<1486:LPHROT>2.3.CO;2), 1999.

Siegert, M. J.: Glacial–interglacial variations in central East Antarctic ice accumulation rates, *Quaternary Science Reviews*, 22, 741–750, 805 [https://doi.org/10.1016/S0277-3791\(02\)00191-9](https://doi.org/10.1016/S0277-3791(02)00191-9), <https://www.sciencedirect.com/science/article/pii/S0277379102001919>, 2003.

Simms, A. R., Lisiecki, L., Gebbie, G., Whitehouse, P. L., and Clark, J. F.: Balancing the last glacial maximum (LGM) sea-level budget, *Quaternary Science Reviews*, 205, 143–153, <https://doi.org/10.1016/J.QUASCIREV.2018.12.018>, <https://www.sciencedirect.com/science/article/pii/S0277379118304074>, 2019.

Small, D., Bentley, M. J., Jones, R. S., Pittard, M. L., and Whitehouse, P. L.: Antarctic ice sheet palaeo-thinning rates from vertical transects of 810 cosmogenic exposure ages, *Quaternary Science Reviews*, 206, 65–80, <https://doi.org/10.1016/J.QUASCIREV.2018.12.024>, <https://www.sciencedirect.com/science/article/pii/S0277379118307728>, 2019.

Smellie, J. L., Rocchi, S., Johnson, J. S., Di Vincenzo, G., and Schaefer, J. M.: A tuff cone erupted under frozen-bed ice (northern Victoria Land, Antarctica): linking glaciovolcanic and cosmogenic nuclide data for ice sheet reconstructions, *Bulletin of Volcanology*, 80, 12, <https://doi.org/10.1007/s00445-017-1185-x>, <http://link.springer.com/10.1007/s00445-017-1185-x>, 2018.

Spector, P., Stone, J., Cowdery, S. G., Hall, B., Conway, H., and Bromley, G.: Rapid Early-Holocene Deglaciation in the Ross Sea, Antarctica, *Geophysical Research Letters*, <https://doi.org/10.1002/2017GL074216>, <http://doi.wiley.com/10.1002/2017GL074216>, 2017.

Stern, T., Baxter, A., and Barrett, P.: Isostatic rebound due to glacial erosion within the Transantarctic Mountains, *Geology*, 33, 221, 815 <https://doi.org/10.1130/G21068.1>, 2005.

820 Stevens, C., Sang Lee, W., Fusco, G., Yun, S., Grant, B., Robinson, N., and Yeon Hwang, C.: The influence of the Drygalski Ice Tongue on
the local ocean, *Annals of Glaciology*, 58, 51–59, <https://doi.org/10.1017/aog.2017.4>, https://www.cambridge.org/core/product/identifier/S0260305517000040/type/journal_article, 2017.

825 Stokes, C. R., Tarasov, L., Blomdin, R., Cronin, T. M., Fisher, T. G., Gyllencreutz, R., Hättestrand, C., Heyman, J., Hindmarsh,
R. C., Hughes, A. L., Jakobsson, M., Kirchner, N., Livingstone, S. J., Margold, M., Murton, J. B., Noormets, R., Peltier, W. R.,
Peteet, D. M., Piper, D. J., Preusser, F., Renssen, H., Roberts, D. H., Roche, D. M., Saint-Ange, F., Stroeve, A. P., and Teller,
J. T.: On the reconstruction of palaeo-ice sheets: Recent advances and future challenges, *Quaternary Science Reviews*, 125, 15–49,
<https://doi.org/10.1016/J.QUASCIREV.2015.07.016>, <https://www.sciencedirect.com/science/article/pii/S027737911530055X>, 2015.

830 Stone, J. O., Balco, G. A., Sugden, D. E., Caffee, M. W., Sass, L. C., Cowdery, S. G., and Siddoway, C.: Holocene deglaciation of Marie
Byrd Land, West Antarctica., *Science* (New York, N.Y.), 299, 99–102, <https://doi.org/10.1126/science.1077998>, 2003.

835 Stuiver, M., Denton, G., Hughes, T., and Fastook, J.: History of the Marine Ice Sheet in West Antarctic during the Last Glaciation: A working
hypothesis, in: *The Last Great Ice Sheets*, edited by Denton, G. H. and Hughes, T., pp. 319–369, Wiley, New York, 1981.

840 Stutz, J.: Reconstruction of LGM and Post LGM Glacial Environment of McMurdo Sound: Implications for Ice Dynamics, Depositional
Systems and Glacial Isostatic Adjustment, Ph.D. thesis, The Ohio State University, 2012.

845 Todd, C., Stone, J., Conway, H., Hall, B., and Bromley, G.: Late Quaternary evolution of Reedy Glacier, Antarctica, *Quaternary Science
Reviews*, 29, 1328–1341, <https://doi.org/10.1016/j.quascirev.2010.02.001>, 2010.

850 van Wessem, J. M., van de Berg, W. J., Noël, B. P. Y., van Meijgaard, E., Amory, C., Birnbaum, G., Jakobs, C. L., Krüger, K., Lenaerts, J.
T. M., Lhermitte, S., Ligtenberg, S. R. M., Medley, B., Reijmer, C. H., van Tricht, K., Trusel, L. D., van Ulft, L. H., Wouters, B., Wuite,
J., and van den Broeke, M. R.: Modelling the climate and surface mass balance of polar ice sheets using RACMO2 – Part 2: Antarctica
(1979–2016), *The Cryosphere*, 12, 1479–1498, <https://doi.org/10.5194/tc-12-1479-2018>, <https://www.the-cryosphere.net/12/1479/2018/>,
2018.

855 Vargo, L. J., Anderson, B. M., Horgan, H. J., Mackintosh, A. N., Lorrey, A. M., and Thornton, M.: Using structure from motion
photogrammetry to measure past glacier changes from historic aerial photographs, *Journal of Glaciology*, 63, 1105–1118,
<https://doi.org/10.1017/jog.2017.79>, https://www.cambridge.org/core/product/identifier/S002214301700079X/type/journal_article, 2017.

860 Veres, D., Bazin, L., Landais, A., Toyé Mahamadou Kele, H., Lemieux-Dudon, B., Parrenin, F., Martinerie, P., Blayo, E., Blunier, T.,
Capron, E., Chappellaz, J., Rasmussen, S. O., Severi, M., Svensson, A., Vinther, B., and Wolff, E. W.: The Antarctic ice core chronology
(AICC2012): an optimized multi-parameter and multi-site dating approach for the last 120 thousand years, *Climate of the Past*, 9, 1733–
1748, <https://doi.org/10.5194/cp-9-1733-2013>, <https://www.clim-past.net/9/1733/2013/>, 2013.

865 Verleyen, E., Hodgson, D. A., Sabbe, K., Cremer, H., Emslie, S. D., Gibson, J., Hall, B., Imura, S., Kudoh, S., Marshall, G. J.,
McMinn, A., Melles, M., Newman, L., Roberts, D., Roberts, S. J., Singh, S. M., Sterken, M., Tavernier, I., Verkulich, S.,
de Vyver, E. V., Van Nieuwenhuyze, W., Wagner, B., and Vyverman, W.: Post-glacial regional climate variability along the East
Antarctic coastal margin—Evidence from shallow marine and coastal terrestrial records, *Earth-Science Reviews*, 104, 199–212,
<https://doi.org/10.1016/J.EARSCIREV.2010.10.006>, <https://www.sciencedirect.com/science/article/pii/S0012825210001418>, 2011.

870 Vieli, A. and Payne, A. J.: Assessing the ability of numerical ice sheet models to simulate grounding line migration, *Journal of Geophysical
Research: Earth Surface*, 110, F01 003, <https://doi.org/10.1029/2004JF000202>, 2005.

875 Walker, C. and Gardner, A.: Changes in East Antarctic Glaciers, in: *AGU Fall Meeting*, Washington, D.C., <https://fallmeeting.agu.org/2018/files/2018/12/PCSlidesAGU2018WalkerGardner.pdf>, 2018.

Weber, M. E., Clark, P. U., Kuhn, G., Timmermann, A., Sprenk, D., Gladstone, R., Zhang, X., Lohmann, G., Menviel, L., Chikamoto, M. O., Friedrich, T., and Ohlwein, C.: Millennial-scale variability in Antarctic ice-sheet discharge during the last deglaciation, *Nature*, 510, 134–138, <https://doi.org/10.1038/nature13397>, <http://www.nature.com/articles/nature13397>, 2014.

Weertman, J., Bentley, C. R., and Walker, J. C. F.: Stability of the Junction of an Ice Sheet and an Ice Shelf, *Journal of Glaciology*, 13, 3–11, 860 <https://doi.org/10.1017/S0022143000023327>, 1974.

White, D. A., Fink, D., and Gore, D. B.: Cosmogenic nuclide evidence for enhanced sensitivity of an East Antarctic ice stream to change during the last deglaciation, *Geology*, 39, 23–26, <https://doi.org/10.1130/G31591.1>, <https://pubs.geoscienceworld.org/geology/article/39/1/23-26/130375>, 2011.

Whitehouse, P. L.: Glacial isostatic adjustment modelling: Historical perspectives, recent advances, and future directions, *Earth Surface Dynamics*, 6, 401–429, <https://doi.org/10.5194/esurf-6-401-2018>, 2018.

Whitehouse, P. L., Bentley, M. J., and Le Brocq, A. M.: A deglacial model for Antarctica: geological constraints and glaciological modelling as a basis for a new model of Antarctic glacial isostatic adjustment, *Quaternary Science Reviews*, 32, 1–24, 865 <https://doi.org/10.1016/j.quascirev.2011.11.016>, 2012.

Whitehouse, P. L., Bentley, M. J., Vieli, A., Jamieson, S. S. R., Hein, A. S., and Sugden, D. E.: Controls on Last Glacial Maximum ice extent in the Weddell Sea embayment, Antarctica, *Journal of Geophysical Research: Earth Surface*, 122, 371–397, 870 <https://doi.org/10.1002/2016JF004121>, 2017.

Whitehouse, P. L., Gomez, N., King, M. A., and Wiens, D. A.: Solid Earth change and the evolution of the Antarctic Ice Sheet, *Nature Communications*, 10, 503, <https://doi.org/10.1038/s41467-018-08068-y>, <http://www.nature.com/articles/s41467-018-08068-y>, 2019.

Wille, J. D., Favier, V., Dufour, A., Gorodetskaya, I. V., Turner, J., Agosta, C., and Codron, F.: West Antarctic surface melt triggered by atmospheric rivers, *Nature Geoscience*, 12, 911–916, <https://doi.org/10.1038/s41561-019-0460-1>, <http://www.nature.com/articles/s41561-019-0460-1>, 2019.

Yokoyama, Y., Anderson, J. B., Yamane, M., Simkins, L. M., Miyairi, Y., Yamazaki, T., Koizumi, M., Suga, H., Kusahara, K., Prothro, L., Hasumi, H., Sounthor, J. R., and Ohkouchi, N.: Widespread collapse of the Ross Ice Shelf during the late Holocene, *PNAS*, 113, 2354–2359, <https://doi.org/10.1073/pnas.1516908113>, 2016.

Zoet, L. K., Anandakrishnan, S., Alley, R. B., Nyblade, A. A., and Wiens, D. A.: Motion of an Antarctic glacier by repeated tidally modulated earthquakes, *Nature Geoscience*, 5, 623–626, <https://doi.org/10.1038/NGEO1555>, 2012.